# GOLF BALL AERODYNAMICS

A dissertation submitted to the University of Manchester
for the degree of Master of Science
in the Faculty of Engineering and Physical Sciences

2014

**James Fielder**
School of Mathematics

# Contents

Word count xxxxx

# List of Tables

# List of Figures

# Abstract

In this project we work on golf balls and stuff.

# Declaration

No portion of the work referred to in the dissertation has been submitted in support of an application for another degree or qualification of this or any other university or other institute of learning.

# Intellectual Property Statement

**i.** The author of this dissertation (including any appendices and/or schedules to this dissertation) owns certain copyright or related rights in it (the "Copyright") and s/he has given The University of Manchester certain rights to use such Copyright, including for administrative purposes.

**ii.** Copies of this dissertation, either in full or in extracts and whether in hard or electronic copy, may be made **only** in accordance with the Copyright, Designs and Patents Act 1988 (as amended) and regulations issued under it or, where appropriate, in accordance with licensing agreements which the University has entered into. This page must form part of any such copies made.

**iii.** The ownership of certain Copyright, patents, designs, trade marks and other intellectual property (the "Intellectual Property") and any reproductions of copyright works in the dissertation, for example graphs and tables ("Reproductions"), which may be described in this dissertation, may not be owned by the author and may be owned by third parties. Such Intellectual Property and Reproductions cannot and must not be made available for use without the prior written permission of the owner(s) of the relevant Intellectual Property and/or Reproductions.

**iv.** Further information on the conditions under which disclosure, publication and commercialisation of this dissertation, the Copyright and any Intellectual Property and/or Reproductions described in it may take place is available in the University IP Policy (see http://documents.manchester.ac.uk/DocuInfo.aspx?DocID=487), in any relevant Dissertation restriction declarations deposited in the University Library, The University Library's regulations (see http://www.manchester.ac.uk/library/aboutus/regulations) and in The University's Guidance on Presentation of Dissertations.

# Acknowledgements

I would like to thank my supervisor Prof. Jitesh Gajjar for his guidance during the project without which I would have been completely lost. Additionally, I would like to thank The R&A for their sponsorship of the project and Dr Steve Otto for his guidance and assistance.

# Chapter 1

# Introduction

Stuff here about the project and aims and such.

## 1.1 A Brief History of Golf

The origins of the game of golf are difficult to trace, with suggestions that the game originated in either Scotland, France, the Netherlands, China, or even going back as far as the Roman Empire. Golf in its more modern incarnation however, is agreed to have originated in the 15th century in Scotland, where the first written records of the game are (somewhat humorously) related to King James II of Scotland banning the game in 1457 for fear of a decrease in archery practice in its favour.

From the 18th century onwards golf began to take form fully in Scotland, with the founding of both The Royal and Ancient Golf Club in St Andrews and The Royal Burgess Golfing Society in Edinburgh. The oldest surviving rules of golf also date from this time and these rules have been in a state of constant revision up to the modern day.

In the 19th century the popularity of golf vastly increased, seeing larger numbers of people knowing and playing the game, and the start of the first major tournaments. Additionally, the game spread out to encompass much of the British empire, to the United States and eventually to Japan, making golf into a global sport supported by a plethora of associated manufacturers, sponsors and organisations.

In the modern day, golf is potentially one of the largest sports on earth, with golf tournaments, golf manufacturing and related industries accounting for hundreds of

billions of pounds of economic activity. If successful on the golf tournament circuit, golf professionals can earn huge sums in prize money. With the players themselves and their sponsors having such a vested interest in success having a consistent and fair rule set is of paramount importance and this is dealt with jointly by The R&A in most of the world and the USGA (United States Golf Association) in the Americas.

## 1.2 A Slightly Larger History of the Golf Ball

Golf ball technology has advanced greatly since the advent of the game. Initially, hard wooden balls were used for playing, however these were soon replaced with featherie balls which are leather pouches stuffed with feathers and then painted white.

The next major innovation in the design of golf balls came in 1848, when the gutta-percha ball was invented. This is the first ball to use a rubbery substance as continues to this day, and was easier to make into a proper sphere, unlike the previous types of ball. It was around this time that it was discovered that abrasions to the surface of the ball would improve the aerodynamic properties of the ball, making it easier to control the flight of the ball and increasing the distance at which the game could be played. This would start a series of innovations that would lead to todays dimpled balls, which we will discuss later.


(a) "Featherie" balls (b) A modern style ball

Figure 1.1: In 1.1a are "Featherie" golf balls, taken from https://en.wikipedia.org/wiki/File:Featherie_golf_ball.JPG, and in 1.1b is a modern style ball.

After this the golf ball once again changed form with the advent of using wrapped rubber thread to help the ball to bounce better. This was coupled with the first usage of a plastic covering, in order to protect the rubber inside the ball on impact with the club. This cover also persists to this day, although the inside of the ball has seen significant development.

The modern golf ball has changed significantly from old designs. The interior of the ball is now usually a 3 piece rubber composite, with different properties in each rubber to maximize the controllability of the ball during play. The exterior is a polyurethane cover (normally white but some are in other colours) with usually between 300 to 400 dimples (though these can go as low as 200 dimples, and beyond 600 in some cases). The properties of the ball are stipulated to be within certain ranges, as set by The R&A and USGA in the rules of golf. The weight of a ball must not be greater than 45.93g, the diameter no less than 42.67mm and the ball must be spherically symmetric.

## 1.3 Aims of the Project

The aim of this project is to obtain a model for how golf balls fly based on an understanding of the fluid mechanics governing the flight of a golf ball. Using this knowledge, we then wish to obtain a simple physical model which describes most, if not all, of the behaviour as the ball flies.

Given this model we then wish to categorise individual balls based on measurements of their flight, and use this categorisation to predict trajectories for the ball based on different initial conditions. Finally, using this model, we will attempt to use a limited set of flight data (between 20 and 30 m) to predict the full flight for the ball.

# Chapter 2

# Preliminary Investigations and Background

In order to devise a simple model for golf ball flight we first must understand some prerequisite physics for projectiles and fluid dynamics for the airflow over the ball. Understanding how the fluid flows over the surface of the ball is crucial to understanding the difference between the flight of a golf ball and that of a standard projectile. Quantifying this effect will be a large component of this project.

There has been significant work done previously in understanding the fluid dynamics around a golf ball and how a golf ball flies. We will attempt to review some of this literature in this chapter and summarise previous work on the topic.

First though, we must understand how normal projectiles fly without taking into account fluid dynamics effects.

## 2.1 Projectile Motion

A projectile is a body fired into the air by an initial impulse and then allowed to fall back to ground under the action of gravity alone. This is the most naive and simplistic model of golf ball flight, completely ignoring all aerodynamic effects, however we must understand it before building up to a more complex model.

Consider motion in a 2 dimensional plane, labelled by $x$ along the horizontal and $y$ along the vertical. A projectile is given an initial speed of the form $\mathbf{V}_0 = (v_x, v_y)$. We set the origin of the coordinate system to be the point at the start of the trajectory,

$(x_0, y_0) = (0, 0)$. In this problem the acceleration $(a_x, a_y)$ on the projectile, after the initial impulse, is constant and of the form

$$a_x = 0, \quad a_y = -g \tag{2.1.1}$$

where $g$ is the acceleration due to gravity. Since the acceleration is constant we can use the standard formulas for motion under constant acceleration to derive the dynamics of the projectile Young and Freedman (2008), which are

$$v = v_0 + at \tag{2.1.2a}$$

$$x = v_0 t + \frac{1}{2}at^2 \tag{2.1.2b}$$

$$v^2 = v_0^2 + 2ax \tag{2.1.2c}$$

$$x = \left(\frac{v_0 + v}{2}\right) t. \tag{2.1.2d}$$

Here $v = |\mathbf{V}|$ is the speed at a time $t$, $x$ is the distance from the origin of the coordinate system, $a$ is the component of the acceleration vector under consideration and $v_0 = |\mathbf{V}_0|$ is the initial speed.

We will write the equations in component form along the axes. Let $\mathbf{V}_0$ be the initial velocity. In component form these will be

$$v_{0x} = v_0 \cos\alpha$$

along the $x$-axis and

$$v_{0y} = v_0 \sin\alpha$$

where $\alpha$ is the angle $\mathbf{V}_0$ makes with the $x$-axis. Now using (2.1.1) and (2.1.2a) we may find

$$v_x = v_0 \cos\alpha \tag{2.1.3a}$$

and

$$v_y = v_0 \sin\alpha - gt. \tag{2.1.3b}$$

Now, using (2.1.2b) (or by integrating (2.1.3) with respect to $t$), we can obtain the standard formulas for the $x$ and $y$ positions during the flight of the projectile:

$$x = (v_0 \cos\alpha)t \tag{2.1.4a}$$

and

$$y = (v_0 \sin\alpha)t - \frac{1}{2}gt^2. \tag{2.1.4b}$$

Eliminating $t$ between these equations demonstrates that projectiles follow parabolic paths, giving

$$y = x\tan\alpha - \frac{g}{2v_0^2\cos^2\alpha}x^2 \tag{2.1.5}$$

for the path of the projectile.

Finally we may use these equations to find the maximum height, range and time of flight for a projectile. The maximum height is obtained when $v_y = 0$ and solving (2.1.3b) with this condition gives

$$t_H = \frac{v_0\sin\alpha}{g}. \tag{2.1.6}$$

The range is obtained by solving for $y = 0$ in (2.1.4b) and selecting the non trivial root for $t$ of

$$t_F = \frac{2v_0\sin\alpha}{g} \tag{2.1.7}$$

where $t_F$ is the time of flight for the projectile. Inserting this into (2.1.4a) gives

$$x = \frac{2v_0^2\cos\alpha\sin\alpha}{g}$$

and recalling that $\sin 2\alpha = 2\cos\alpha\sin\alpha$ gives

$$x = \frac{v_0^2\sin 2\alpha}{g} \tag{2.1.8}$$

for the range of the projectile.

### 2.1.1 3D Projectile Motion

Projectile motion in 3 dimensions works in exactly the same fashion as 2D projectile motion. Here we will take the $z$-axis to be the vertical and $x$ and $y$ axes to be labelling the surface. The only component of acceleration is along the $z$-axis, with

$$a_z = -g$$

as before. All other equations remain the same.

## 2.2 Basic Aerodynamics

Of course, the flight of a golf ball is inevitably affected by aerodynamics. As such we need to have some understanding of how aerodynamic effects will manifest themselves during the flight of the ball. In particular, we will need to understand how boundary layers form on and separate from the surface of the golf ball and how this effects the lift and drag on the ball. First we will review some basic fluid mechanics.

### 2.2.1 Fluid Mechanics

In this project we will model the air flowing around the ball as being an incompressible fluid. We will consider an Eulerian description of fluid flow, viewing the motion as though the ball is fixed in the centre of the coordinate system and the fluid moving around the ball Ruban and Gajjar (2014).

We will not concern ourselves with a full discussion of fluid mechanics from basic principles here, instead we will simply state some useful results predominantly following Ruban and Gajjar (2014) and Sears (2011).

Let $\mathbf{V}$ be the fluid velocity, which is a function of the the position $\mathbf{r}$ from the origin of the coordinate system and of time $t$. Let $\rho$ be the density of the fluid and $p$ the pressure. We define the material derivative to be (as a differential operator)

$$\frac{D}{Dt} = \frac{\partial}{\partial t} + (\mathbf{V} \cdot \nabla).$$

This derivative represents the rate of change of some quantity within the fluid, while moving with a small element of the fluid flow. That is, in a description where the fluid moves relative to the coordinate system the material derivative measures the rate of change as seen by a moving fluid element.

At all points within the fluid the mass continuity equation must apply

$$\frac{D\rho}{Dt} + \rho \nabla \cdot \mathbf{V} = 0. \tag{2.2.1}$$

This equation encodes the condition that mass is conserved within a fluid without any sources or sinks. In an incompressible fluid, as we will be primarily conserved with in this project, $\rho$ will not change with time, and as such $D\rho/Dt = 0$. As a consequence, both terms on the left hand side of (2.2.1) must be zero everywhere within the fluid,

and therefore the equation reduces to

$$\nabla \cdot \mathbf{V} = 0 \tag{2.2.2}$$

for an incompressible fluid.

The continuity equation gives one equation for the velocity components $u, v, w$[1] within a fluid. In order to specify the pressure and velocity everywhere we therefore require three more equations to determine the system. These three equations are supplied by considerations of energy and momentum conservation. Keeping all of these in mind, we may write a momentum equation in the form

$$\rho \frac{D\mathbf{V}}{Dt} = -\nabla p + \mu \nabla^2 \mathbf{V} + \mathbf{f} \tag{2.2.3}$$

where $\mathbf{f}$ is body force per unit volume acting on the fluid (for example a gravitational force) and $\mu$ is the viscosity of the fluid.

Equations (2.2.2) and (2.2.3) when taken together form the Navier-Stokes equations for the velocity and pressure fields within an incompressible fluid. It is well known that these equations are highly non-linear and exceedingly difficult to solve both analytically and numerically, except in special circumstances.

From solutions of the Navier-Stokes equations emerges a number of fascinating effects within fluid dynamics. In this project, we are particularly interested in boundary layer effects and turbulence.

### 2.2.2 Non Dimensional Variables and the Reynolds Number

In physics we are often interested in understanding the behaviour of a system independent of a choice of units Misic et al. (2010). Instead, we wish to have a system of measurement which does not depend intrinsically on one set on units, but on more fundamental ideas such as length or mass. We desire this for two main reasons:

- Physical statements should not have any dependency on the units they are stated in. Non-dimensionalising the problem ensures that this is the case.

[1] The convention within fluid mechanics is that the $x, y, z$ velocity components are called $u, v, w$ respectively. That is

$$v_x = u, \qquad v_y = v, \qquad v_z = w.$$

- Using non-dimensional variables allow problems of different scales to be compared to each other on an equal footing. Often the points when the physical behaviour of the system changes will depend on some non-dimensional parameter, as we will see with turbulence later.

Additionally, analysing the fundamental dimensions of a physical problem can yield information on the functional form of quantities within the model without having to use more advanced mathematical techniques to derive such results. By simply understanding the dependency on fundamental units we often can find interesting scaling laws for functions of interest.

The fundamental dimensions (only those which will be useful in this project) are as follows:

| Dimension | Symbol |
|---|---|
| Length | $L$ |
| Mass | $M$ |
| Time | $T$ |

Table 2.1: List of fundamental dimensions we will require in this report.

Any quantities of interest can be written using these variables: for example, an area $A$ would have the dimensions $[A] = L^2$ and a velocity $[V] = L/T$.

Physical laws can, in general, be written as, Misic et al. (2010)

$$q_0 = f(q_1, q_2, \ldots, q_n) \tag{2.2.4}$$

where $q_0$ is a physical quantity we are interested in obtaining, $q_1, \ldots, q_n$ are independent physical quantities and $f$ is a functional relationship between them.

When analysing the dimensions of a problem we must ensure that the following conditions are satisfied

- Both sides of (2.2.4) must have the same fundamental dimensions.
- Any sum of $q_i$ must have the same dimensions.
- Any function of $q_i$ (say, exponential or trigonometric) must be dimensionless. This is as a direct result of the last condition and being able to expand these functions as a power series.

We will demonstrate this technique in section 2.2.4.

One of the aims of dimensional analysis is to find groupings of physical quantities which are dimensionless. These have useful properties of scale invariance which leads to natural parameterisations for physical problems. A key result in finding such dimensionless groupings is the Buckingham $\pi$ theorem, which states the following:

**Theorem 1** (Buckingham $\pi$)**.** *Consider a physical law in the form of* (2.2.4)*. Let there be $n$ parameters $q_1, q_2, \ldots, q_n$, and $k$ fundamental units in which these parameters may be written. Then there exist $n-k$ dimensionless parameters $\pi_i$ which satisfy*

$$F(\pi_1, \ldots, \pi_{n-k}) = 0$$

*for some function $F$.*

Within fluid mechanics one such dimensionless grouping which manifests often is the Reynolds number, defined as

$$Re = \frac{\rho v L}{\mu}. \tag{2.2.5}$$

For a sphere, $v, \mu$ and $\rho$ are defined as they have already been in this text, and the characteristic length $L$ is defined to be the diameter of the sphere. The Reynolds number represents the ratio of inertial forces to viscous ones, and we will make considerable use of it within the project. The Reynolds number, in some ways, can be considered to be a non dimensional analogue of the velocity, taking into account the intrinsic length scale of the problem under consideration.

### 2.2.3 Boundary Layers

One of the fundamental ideas within fluid mechanics is that of the no slip condition. The no slip condition specifies that when a fluid encounters a solid body it must, at the surface of the body, take the velocity and temperature of that body.

The concept of the boundary layer was introduced by Ludwig Prandtl in 1904 at the International Mathematics Congress. Initially the utility of the ideas Prandtl presented were not appreciated, however Prandtl's ideas have shaped fluid mechanics in the century after his work was presented.

For high Reynolds numbers the flow can be divided into two portions: the free stream flow where the fluid moves quickly and viscous effects are unimportant, and

a thin layer of fluid around the body called the boundary layer where viscous effects come into play. The origin of this thin layer of fluid is the no slip condition: at the surface of the body the fluid must take the velocity of the body itself. However, as we move away from the body the fluid very quickly returns to the free stream velocity. The domain over which this rapid change in velocity occurs is the boundary layer.

The equations which govern the flow within the boundary layer are a simplified version of the Navier-Stokes equations, taking into account the order of magnitude of the boundary layer compared to the size of the body. The derivation of these equations completed by scaling the Navier-Stokes based on the assumption that the boundary layer is much smaller than the body size Anderson (1985).

Boundary layer theory has been hugely important in the development of aerodynamics, taking previously intractable problems and facilitating a better understanding of the fluid dynamics of bodies Anderson (1985). The affect of the boundary layer will be important in the modelling of golf balls, as we will see later.

### 2.2.4 Lift and Drag

In order to go beyond modelling golf ball flight as simply that of a projectile we must understand how the lift and drag forces affect the flight of the ball. We can use dimensional analysis arguments to obtain a functional form for these effects. Here we follow the analysis of Misic et al. (2010) and Anderson (1985) in order to demonstrate the analysis for the drag force. The lift is found in a similar way.

One first must ask what physical terms we would expect the drag to have a dependency on. We would expect some dependency on the velocity $v$ of the object through the fluid, on the shape of the body and a characteristic length scale $r$ for the body, on the density of the fluid $\rho$, and finally on the viscosity of the fluid $\nu$.

Forming an equation in the style of (2.2.4) between these quantities and the drag force $D$ we obtain

$$D = kf(v, r, \rho, \nu) \tag{2.2.6}$$

where $k$ is a dimensionless constant which will take into account the shape of the body and potentially other dimensionless parameters such as the Reynolds number (2.2.5).

We attempt to obtain values of $\alpha, \beta, \gamma, \delta$ which balances (2.2.6). The dimensions of

the quantities in (2.2.6) are as follows:

$$[D] = MLT^{-2}, \qquad [v] = LT^{-1}, \qquad [r] = L, \qquad [\rho] = ML^{-3}, \qquad [\nu] = ML^{-1}T^{-1}$$

and so balancing (2.2.6) implies that

$$MLT^{-2} = M^{\gamma+\delta}L^{\alpha+\beta-3\gamma-\delta}T^{-\alpha-\delta}. \tag{2.2.7}$$

Equating the powers leads to a system of 3 linear equations in 4 variables for each fundamental unit given by

$$1 = \gamma + \delta \tag{2.2.8a}$$

$$1 = \alpha + \beta - 3\gamma - \delta \tag{2.2.8b}$$

$$-2 = \alpha - \delta \tag{2.2.8c}$$

for $M, L$ and $T$ respectively.

Using these equations we can eliminate all but one of the parameters, and by application of the Buckingham $\pi$ theorem we expect that there will be $4 - 3 = 1$ dimensionless parameters. Writing all these in terms of $\delta$ we can find

$$D = kv^{2-\delta}r^{2-\delta}\rho^{1-\delta}\nu^{\delta} \tag{2.2.9}$$

and rearranging these powers

$$D = k\rho r^2 v^2 \left(\frac{\nu}{\rho r v}\right)^{\delta}. \tag{2.2.10}$$

We can then recognise that the term in the brackets is $1/Re$. Since the Reynolds number is raised to an arbitrary power $\delta$ we can include the constant $k$ and the $Re^{-\delta}$ into one functional form, $f(Re)$, which accounts for the dimensionless factor. Writing into this form gives

$$D = f(Re)\rho r^2 v^2. \tag{2.2.11}$$

Notice that now we have $[D] = [\rho r^2 v^2] = MLT^{-2}$ as we expect. The form of $f$ depends on the velocity of the body moving through the fluid.

There are two separate cases of drag which occur in nature. The low Reynolds number case and the high Reynolds number case. In this project we will be concerned with the high Reynolds number case, where drag takes the form of (2.2.11). However, in the low Reynolds number case the form of the drag is Misic et al. (2010)

$$D = k\nu r v \tag{2.2.12}$$

which is known as Stokes drag. We will not consider this form in this project.

Within the literature related to fluid dynamics and aerodynamics (2.2.11) is normally written with different names for the variables, namely

$$F_D = \frac{1}{2}\rho \mathbf{V}^2 A c_D \tag{2.2.13}$$

where $F_D$ is the drag force, and $c_D$ is the dimensionless drag coefficient which depends on the Reynolds number. It is this form we will use from here on.

An expression for the lift can be derived using very similar analysis, and has the same form as the drag:

$$F_L = \frac{1}{2}\rho \mathbf{V}^2 A c_L \tag{2.2.14}$$

where here $c_L$ is the lift coefficient.

### 2.2.5 Boundary Layer Separation

Boundary layer separation is a phenomena whereby the boundary layer of an object "peels" away from the body and forms a wake behind the body. The idea of boundary layer separation was also introduced by Prandtl in 1904 at the same time as presenting his initial work on boundary layers.

The mechanism by which this occurs is the flow in the boundary layer moving against an adverse pressure gradient. As the fluid in the boundary layer moves against the adverse pressure gradient, the speed of the fluid slows until eventually coming to a complete stop and then proceeding back in the direction it arrived. At this point the fluid moves away from the body, expanding the boundary layer at the separation point beyond the usual thickness of the layer.

The fluid which has detached from the body then begins to form vortices in the wake behind the body, increasing the drag on the body considerably as the pressure at the front and back of the body changes considerably.

### 2.2.6 The Magnus Effect

In addition to the drag forces which we have discussed in the previous section, there is another major effect from the motion of the fluid on golf ball trajectories: the Magnus effect. The Magnus effect is caused by the spin of the ball moving through the fluid

medium, and accounts for large deviations from a trajectory not considering the effect Seifert (2012).

In the Magnus effect, the boundary layer around the spinning body separates from the body at different points and forms a wake behind the body which does not point in the direction of motion.

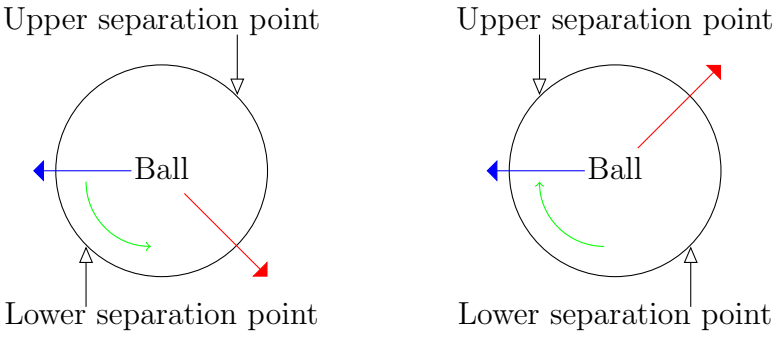


(a) Boundary layer separation

(b) Reversed boundary layer separation

Figure 2.1: Here we see the two scenarios for boundary layer detachment. The red arrow indicates the direction which the detached boundary layer proceeds in, the blue the direction of the ball, and the green arrow the direction of spin of the ball.

The points at which the boundary layer separates from the body at the top and bottom of the ball make a significant difference to the direction in which the wake will point: if the boundary layer at the top of the ball separates later than the bottom (see Figure 2.1a) then we will have a positive Magnus effect, and the lift will be increased. In the opposite case, where the bottom separates later than the top, we will have a negative Magnus effect (see Figure 2.1b) and the lift on the ball will be decreased or potentially act to push the ball further towards the ground.

The fluid behind the rotating sphere will become turbulent as the sphere leaves a gap which the wake refills as it passes. This mechanism is important while modelling the golf ball later, as the size of the turbulent wake will affect the drag on the ball.

In Figure 2.2 we see a representation of the streamlines over a sphere. Here we have laminar flow in the boundary layer. However this is not always the case, if the flow is turbulent within the boundary layer before separation the drag can change considerably.

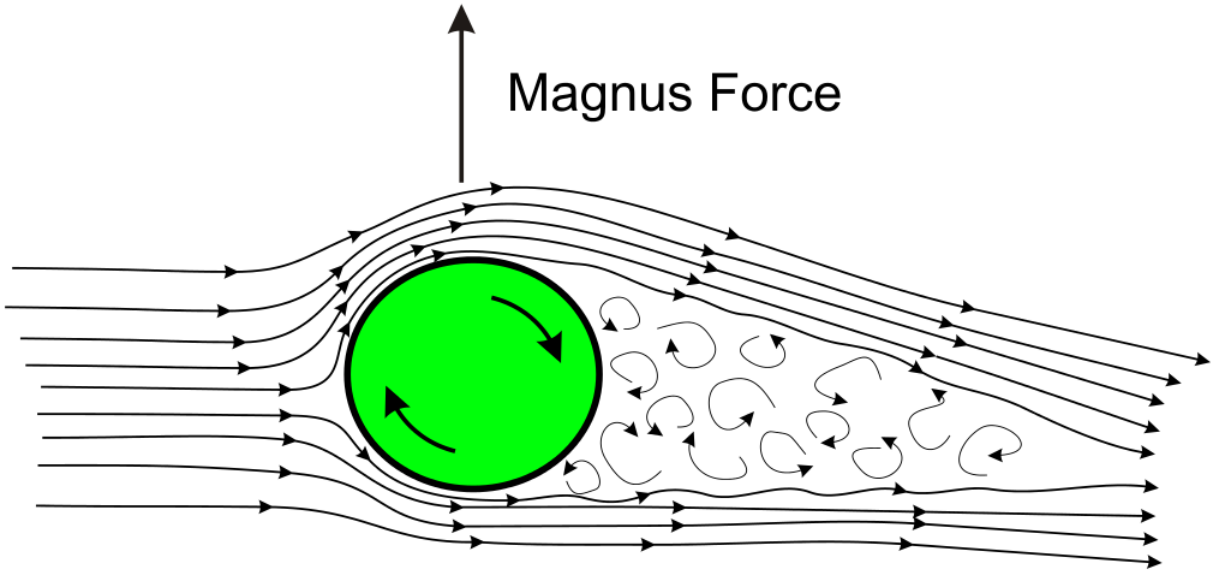


Figure 2.2: A diagram of the Magnus force on a rotating sphere. Adapted from http://en.wikipedia.org/wiki/File:Sketch_of_Magnus_effect_with_streamlines_and_turbulent_wake.svg.

### 2.2.7 The Drag Crisis

When measuring the flow around a smooth sphere, one finds a curious phenomenon. At approximately $Re = 2 \times 10^5$ the drag coefficient on the sphere suddenly decreases from around $c_D = 0.4$ to $c_D = 0.1$. This sudden change in drag is associated with the boundary layer around the sphere becoming turbulent and the wake behind the ball, as described before, becoming shorter and thinner as compared to the size of the ball.

Modelling this transition to turbulence is incredibly difficult, even for smooth spheres, and is incredibly difficult for the case of a dimpled golf ball. We must make do with measurements from experiments to understand the behaviour of $c_D$ as the Reynolds number varies.

In Morrison (2010) all experimental data for the drag on a smooth sphere is combined to give a formula for the drag in the Reynolds number range $Re = 1$ to $Re = 10^6$. This combined form exhibits the drag crisis drop at around $Re = 2 \times 10^5$ experiments have seen, and is given by

$$c_D = \frac{24}{Re} + \frac{2.6(Re/5)}{1 + (Re/5)^{1.52}} + \frac{0.411(Re/263000)^{-7.94}}{1 + (Re/263000)^{-8.00}} + \frac{Re^{0.8}}{461000}. \tag{2.2.15}$$

using experimental results found from Schlichting (1968).

For a golf ball, the presence of dimples on the surface of the ball serves to reduce the Reynolds number at which the drag crisis occurs Bearman and Harvey (1976),

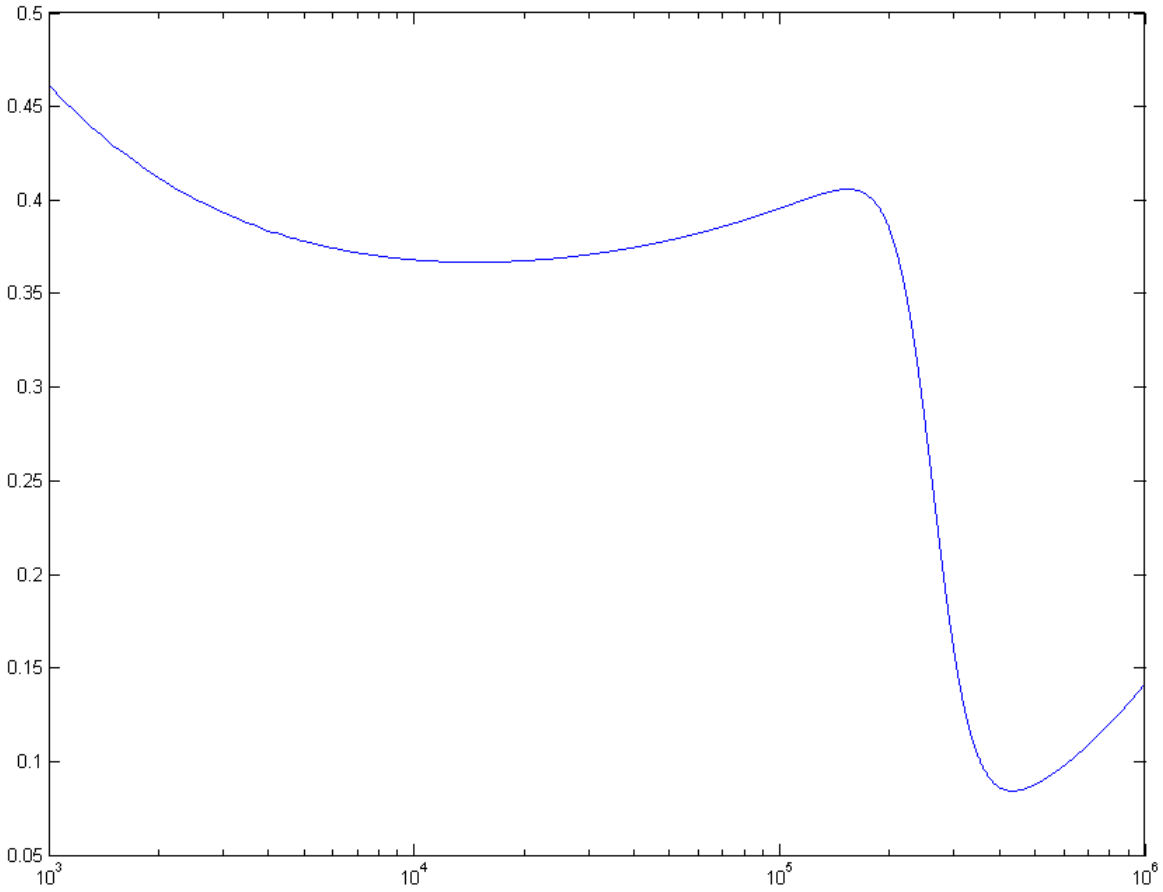


Figure 2.3: A plot of the Morrison drag formula from $Re = 10^3$ to $Re = 10^6$. Note the sudden drop in drag at around $Re = 2 \times 10^5$ as expected.

moving the range of speeds where the golf ball is in the low drag (supercritical) region to within the capability of a human golfer to hit. This vast reduction in drag makes a large difference to the flight of a ball, and we will need to account for this affect in any model we form.

The mechanism by which this reduction in drag occurs is the boundary layer around the body becoming turbulent. This turbulence delays boundary layer separation (keeping the layer on the body closer to the back) and thus reduces the size of the wake which results when the boundary layer separates. Reducing the size of the wake has the effect of reducing the pressure difference between the front of the body and the back, overall reducing the drag.

The configuration of the dimples on the ball also has a large effect on the values of $Re$ at which the drag crisis occurs, and the value of $c_D$ at either side of the drop Naruo and Mizota (2014). The dimples serve to introduce vortices, and thus encourage

turbulence, at a lower value of Reynolds number. There is a large variation between particular type of ball (see Figure 3 in Naruo and Mizota (2014)), which mean that individual balls can likely be characterised simply in terms of their drag function.

## 2.3 Previous Work on Modelling Golf Ball Flight

There has been considerable attention within the literature on the topic of modelling the flight of a golf ball, both due to the considerable industry surrounding the game and the interesting fluid dynamics which results from golf ball flight. A small selection of such papers are Smits and Ogg (2004); Bearman and Harvey (1976); Penner (2003); Alam et al. (2011); Kensrud and Smith (2010); Leong and Lin (2007) however there are many more which could be discussed.

The earliest of these papers is Bearman and Harvey (1976) which is one of the first attempts to understand the fluid dynamics over a golf ball and provide a model for the flight of a ball taking this into account. The drag crisis on a golf ball is shown in experimental data taken from an earlier paper and from measurements the authors made in a wind tunnel. These measurements were taken at a range of $Re$ values and spin values, providing a useful set data to correlate any findings against. The paper also emphasizes the importance of the dimples on the aerodynamic characteristics of the ball, in agreement with other papers.

In Smits and Ogg (2004) the authors summarise the main effects one will find on golf ball trajectories, mentioning both the laminar and turbulent boundary layer we discussed previously, the effect of spin on the lift coefficient, and including some of the data from Bearman and Harvey (1976) to illustrate these points. The paper also suggests that much work still remains in understanding how the fluid dynamics over golf balls functions, saying that fundamentally balls are designed via empirical means, simply using the knowledge contained in the previous sections and experiments to improve the designs of balls. The authors state also state, with reference to the design of golf balls Smits and Ogg (2004, page 10):

"The fundamental design challenge in optimizing golf ball aerodynamics is achieving the lower possible drag level at high Reynolds number while ensuring a high lift coefficient at the lowest Reynolds number in the design space."

These two goals are virtually at opposite ends from each other and thus means the challenge of making a good golf ball for all ranges of speed in a typical game is very difficult.

There are a number of papers exclusively on experimental measurements of drag and lift on golf balls, for example Bearman and Harvey (1976), Kharlamov et al. (2007), Naruo and Mizota (2014), Kray et al. (2012) and Aoki et al. (2010). All of these papers show evidence for the drag crisis at lower Reynolds number than a smooth sphere, and for the Magnus effect on on flight. Aoki et al. (2010) gives a value for the transition to the supercritical drag regime as $Re = 0.5 \times 10^5$ which is slightly lower than the values given in other references. However, this can be accounted for by noting that this measurement is taken without rotation and potentially with a different ball to other references. Additionally, this paper contains direct measurements of the boundary layer separation on both sides of a rotating ball, and finds excellent agreement between the expected behaviour and the real physical behaviour.

Kray et al. (2012) focuses on the Magnus effect predominantly, and takes experimental measurements on larger spheres than a golf ball. However, these measurements are in a similar Reynolds number range to the case for golf and so the results here could be of some use. The authors also report observing the negative Magnus effect in their tests. However, some of the results within in this report are obtained using a sphere attached to two rods in a wind tunnel which could significantly affect the fluid flow in the boundary layer, a point the authors themselves concede.

Finally, in Naruo and Mizota (2014) the effects of differing the depth of the dimpling on a golf ball is explored at a range of flow speeds. The authors find that even small changes to the dimple configuration (a change in depth of 0.035mm) can have large effects on the lift on the ball and thus the resultant trajectory. Additionally, the authors attempt a strategy with a ball with smaller dimples placed between the normal sized dimples a standard golf ball. They report a increase in the carry of the ball of approximately 8m. While we will not investigate into the dimpling on the ball, it is interesting to see the directions that golf ball technology may advance in the future.

### 2.3.1 Computational Simulations of Golf Ball Flight

Performing accurate computational simulations of the flow over a golf ball is a particularly large challenge. The complex turbulent wake behind a golf ball, and the potential for the turbulent boundary layer, along with the rotation and high Reynolds numbers the flow typically operate in mean that any computational simulations will need both small time stepping and large mesh sizes to deal with the resultant flow.

It is only recently that such simulations have become feasible using super computers with large numbers of cpu cores and memory. Parallelisation of these methods means that systems with large numbers of cpu cores can dramatically cut down the time that such simulations take.

The first paper to attempt a full simulation of the flow over a non spinning ball for a range of Reynolds numbers was Smith et al. (2010). The authors use a fairly sophisticated discretisation method for the points within the domain, dividing them into interior points within the ball, forcing points directly on the boundary which have different boundary conditions, and fluid points. Each of these has different behaviour to the other, and some interpolation methods are used to bridge the gap between the values at each set of points. This methodology is used as the points do not have to fit around the boundary of the ball, allowing a much simpler Cartesian grid to be used instead of attempting to use a grid set in a spherical coordinate system with the ball.

The solution is based on solving the full Navier Stokes equations, (2.2.2) and (2.2.3) around the golf ball for the flow, using a Crank-Nicholson method for the viscous terms and using a third order Runge-Kutta scheme for the other terms. The ball modelled has 300 dimples, a fairly typical configuration.

The results are in good line with the behaviour we expect to see for Reynolds numbers between the subcritical (here $Re = 2.5 \times 10^4$) and supercritical ($Re = 1.1 \times 10^5$) regimes, finding the drag crisis drop that experiments have observed. The authors also obtain visualisations of the flow over the ball in the two different regimes, finding the transition to turbulence in the boundary layer in the supercritical range and the turbulent wake behind the ball.

Beratlis et al. (2012) extends this work to spinning golf balls, and samples from a different set of Reynolds number, this time in the subcritical domain $Re = 1.7 \times 10^4$, during the critical Reynolds number drop $Re = 4.5 \times 10^4$ and $Re = 6.5 \times 10^4$, and in

the supercritical section at $Re = 1.7 \times 10^5$. This study uses a more sophisticated grid setup in cylindrical coordinates, with a similar hybrid explicit and implicit scheme to solve the Navier-Stokes equations around the ball.

The computational resources used within this study are quite considerable: at the lowest Reynolds number considered the grid size is approximately $3 \times 10^7$ points, and the authors estimate that each rotation takes 1800 hours of cpu time to compute. By the final and largest Reynolds number considered, and at highest spin, the grid is increased by over 5 times to approximately $1.5 \times 10^8$ points, and the authors estimate this takes 260000 hours of cpu time to compute.

These investigations find a similar result to both the experiments and the previous work in Smith et al. (2010), seeing all the features we would expect and following the experimental data quite closely.

Finally, in Aoki et al. (2010) some numerical simulations of the flow using the FLUENT fluid dynamics software is undertaken. The authors only obtained a few results, and crucially only one result after the advent of the drag crisis. While the results they find are broadly within line with the expected experimental results there are too few to really validate the accuracy of the technique.

Using computational fluid modelling over golf balls is still in its infancy, and there is a long way to go until the technique is sufficiently accurate to be able to easily model different types of ball. The huge computational resources required are a problem, however as computers grow more powerful and generally have more cores this will come within the range of researchers to quickly simulate the flow over a ball.

## 2.4 Measuring Golf Ball Trajectories

Golf ball trajectories can be measured in a number of ways, depending on the distance over which we wish to take the measurements. There are setups over small ranges which use cameras to track the ball during its flight, however these are limited in the range at which the ball can be distinguished by the camera.

In this project, the data we have been supplied with predominantly uses Doppler radar to measure the full trajectory of the flight. This allows both the position of the ball over the flight to be found and the spin, by virtue of the use of the Doppler effect

to measure the rotational motion of the ball.

It is possible to also use this Doppler radar technique to estimate the $c_D$ at each point of the flight, as is described in Martin et al. (2012) for the case of baseballs.

## 2.5 Summary

The fluid dynamics occurring during golf ball flight is highly complex, with a number of different affects present during the flight. We have considered only the main affects on a spinning sphere which manifest themselves during golf ball flight. There are other phenomena which could be discussed, for example the Basset force, which we have not considered.

Understanding the form which $c_D$ and $c_L$ take for a golf ball is a large part of this project. From the fluid mechanics we have considered in chapter we note that we will expect these functions to depend on the Reynolds number, and for the lift to additionally have some dependency on $\omega$ the angular velocity of the ball.

Understanding the exact nature of the fluid mechanics on each and every ball is still incredibly difficult with the turbulent flow over the ball. As such, any parametrisations of the golf ball characteristics will inevitably be an approximation to the true nature of how this system works.

# Chapter 3

# A Model of Golf Ball Flight

The motion of a golf ball can fundamentally be viewed as a set of forces acting on the ball as it flies through the air. Before we can obtain a better understanding of the nature of the drag and lift, or characterise a ball by the lift and drag functions we find, obtaining a model for the forces acting on the ball during the flight is advisable.

Here, we follow the paper by Robinson and Robinson (2013), which builds a model of the flight based on simple principles as we desire. The equations described within Robinson and Robinson (2013) are not new however: very similar equations appear in Bearman and Harvey (1976). However, the analysis and presentation in Robinson and Robinson (2013) is particularly clear, so we will use this as our starting point.

This model does neglect some of the subtlety of the fluid dynamics we have discussed, but is a useful starting point for the analysis.

## 3.1 A Model for Golf Ball Flight

In Robinson and Robinson (2013) the authors first discuss the assumptions and limitations of the model at hand. We will take the reverse to this approach, discussing the features of the model and then mentioning some of the potential improvements to the model and the drag and lift form they give.

Additionally, the authors give a sample MATLAB script for the setup of the differential equations they derive and suggest using MATLAB to solve the resultant differential equations of the model numerically. This sample code forms the bases of our initial investigations into the trajectories.

### 3.1.1 Lift and Drag

Robinson and Robinson start by initially discussing the lift and drag forces on a golf ball. They use the form of the lift and drag in the high Reynolds number limit, given by

$$F_D = \frac{1}{2}\rho \mathbf{V}^2 A c_D$$

and

$$F_L = \frac{1}{2}\rho \mathbf{V}^2 A c_L$$

The use of this form of equation is justified by the authors stating that there is experimental evidence that golf ball flight always occurs at $Re > 10^3$. We will examine this assumption later.

#### Drag

The authors give a form for $c_D$ based on the spin of the ball

$$c_D = 0.3 + 2.58 \times 10^{-4}\omega \tag{3.1.1}$$

where $\omega$ is the modulus of $\vec{\omega}$ the angular velocity vector, in radians per second. This is obtained from experimental results found by Davies (1949). However, the authors elect to take $c_D = 0.45$, rationalising that this simplification is most suited to the range of spins and speeds which golf balls are likely to take. The authors also mention the lack of experimental evidence they found to suggest better forms for $c_D$.

#### Lift

Robinson and Robinson make the following assumptions for the lift on the golf ball:

- The direction of the lift for is perpendicular to both $\vec{\omega}$ and $\mathbf{V}$, that is $\vec{F_L} \propto \vec{\omega} \times \mathbf{V}$.
- The lift is not a function of the drag.

They then go on to express the lift force as a vector quantity, given by

$$\vec{F_L} = \frac{1}{2}\rho A c_L V^2 \sin\theta \cdot \hat{n} \tag{3.1.2}$$

and then using the definition of cross products rewrite this as

$$\vec{F}_L = \frac{1}{2}\rho A c_L V \cdot \left(\frac{\vec{\omega} \times \mathbf{V}}{\omega}\right) \tag{3.1.3}$$

which is the form used in the model.

As with $c_D$, the authors then use experimental data to inform their choice for $c_L$, once again following Davies (1949) to find that

$$c_L = 3.19 \times 10^{-1} \left(1 - \exp(-2.48 \times 10^{-3}\omega)\right) \tag{3.1.4}$$

fits with a number of different experimental studies of the lift over spheres.

The authors also state that this form completely omits any possibility of a negative Magnus effect pushing the ball towards the ground.

### 3.1.2 Accounting for the Wind

In order to deal with the effect of the wind on the golf ball the authors introduce a new $\vec{v}$ which is defined as being the velocity of the ball relative to the air. That is, if the wind is blowing with a velocity $\vec{W}$ and the ball moving with velocity $\mathbf{V}$ with respect to the coordinates then the ball is moving with velocity $\vec{v} = \mathbf{V} - \vec{W}$ with respect to the air.

### 3.1.3 The Equations of Motion

By considering a force balance on the golf ball in flight, the authors obtain

$$m\ddot{\vec{r}} = \underbrace{-\frac{1}{2}\rho A c_D |\mathbf{V} - \vec{W}|(\mathbf{V} - \vec{W})}_{1} + \underbrace{\frac{1}{2}\rho A c_L |\mathbf{V} - \vec{W}| \left(\frac{\vec{\omega} \times (\mathbf{V} - \vec{W})}{\omega}\right)}_{2} + \underbrace{m\vec{g}}_{3}. \tag{3.1.5}$$

Where $\vec{r}$ is the position vector from the origin, taking the $z$-axis to be facing upwards, and $x$ and $y$ in the plane with the ground. The dot here means the time derivative. The three terms here are numbered by their origin:

1. The drag term accounting for the action of the wind.

2. The lift term, written in terms of cross products, accounting for the action of the wind.

3. The action of gravity on the ball, with $\vec{g} = (0, 0, -g)^T$.

If we write these into their respective components we obtain, expanding the cross product terms into the components of vectors

$$m\ddot{x} = -\frac{1}{2}\rho A|\mathbf{V} - \vec{W}|\left(c_D(V_x - W_x) - c_L\frac{\omega_y(V_z - W_z) - \omega_z(V_y - W_y)}{\omega}\right) \quad (3.1.6a)$$

$$m\ddot{y} = -\frac{1}{2}\rho A|\mathbf{V} - \vec{W}|\left(c_D(V_y - W_y) - c_L\frac{\omega_z(V_x - W_x) - \omega_x(V_z - W_z)}{\omega}\right) \quad (3.1.6b)$$

$$m\ddot{z} = -\frac{1}{2}\rho A|\mathbf{V} - \vec{W}|\left(c_D(V_z - W_z) - c_L\frac{\omega_x(V_y - W_y) - \omega_y(V_x - W_x)}{\omega}\right) - mg. \quad (3.1.6c)$$

In order to solve these equations we rewrite them into a set of 6 first order equations, instead of three second order ones, as

$$\dot{\vec{r}} = \vec{v} \quad (3.1.7a)$$

$$m\dot{\vec{v}} = -\frac{1}{2}\rho A c_D|\mathbf{V} - \vec{W}|(\mathbf{V} - \vec{W}) + \frac{1}{2}\rho A c_L|\mathbf{V} - \vec{W}|\left(\frac{\vec{\omega} \times (\mathbf{V} - \vec{W})}{\omega}\right) + m\vec{g} \quad (3.1.7b)$$

This rewriting allows an implementation of the equations which may be integrated using the standard differential equation solvers within MATLAB.

Solving these equations involves giving 6 initial conditions and 3 parameters: the three coordinates at the start of the trajectory, the components of the initial velocity, $\rho = 1.22\text{kg}\,\text{m}^{-3}$ in air, the diameter of the ball ($D = 42.67\text{mm}$[1]), and the angular velocity vector of the ball.

We will also assume that $\omega_x = 0$, that is the rotation of the ball is always "towards" the $x$-axis and thus only $\omega_y$ and $\omega_z$ are none zero. We will specify these components as $\omega_y = |\vec{\omega}|\cos\theta$ and $\omega_z = |\vec{\omega}|\sin\theta$ where $\theta$ is an angle measuring the tilt of the spin axis from the $x$-$y$ plane.

### 3.1.4 An Example Trajectory

In order to show this model working, we will demonstrate solving an example problem in matlab with values taken from a trajectory provided by The R&A.

Here, we take the following initial conditions

$$x = 0,\ y = 0,\ z = 0,\ v_x = 68.221,\ v_z = 12.701,\ v_y = -4.961,\ |\vec{\omega}| = 271.44,\ \theta = \frac{169\pi}{180}$$

[1]This is the size of the largest ball allowed by The R&A, as was stated in the introduction.

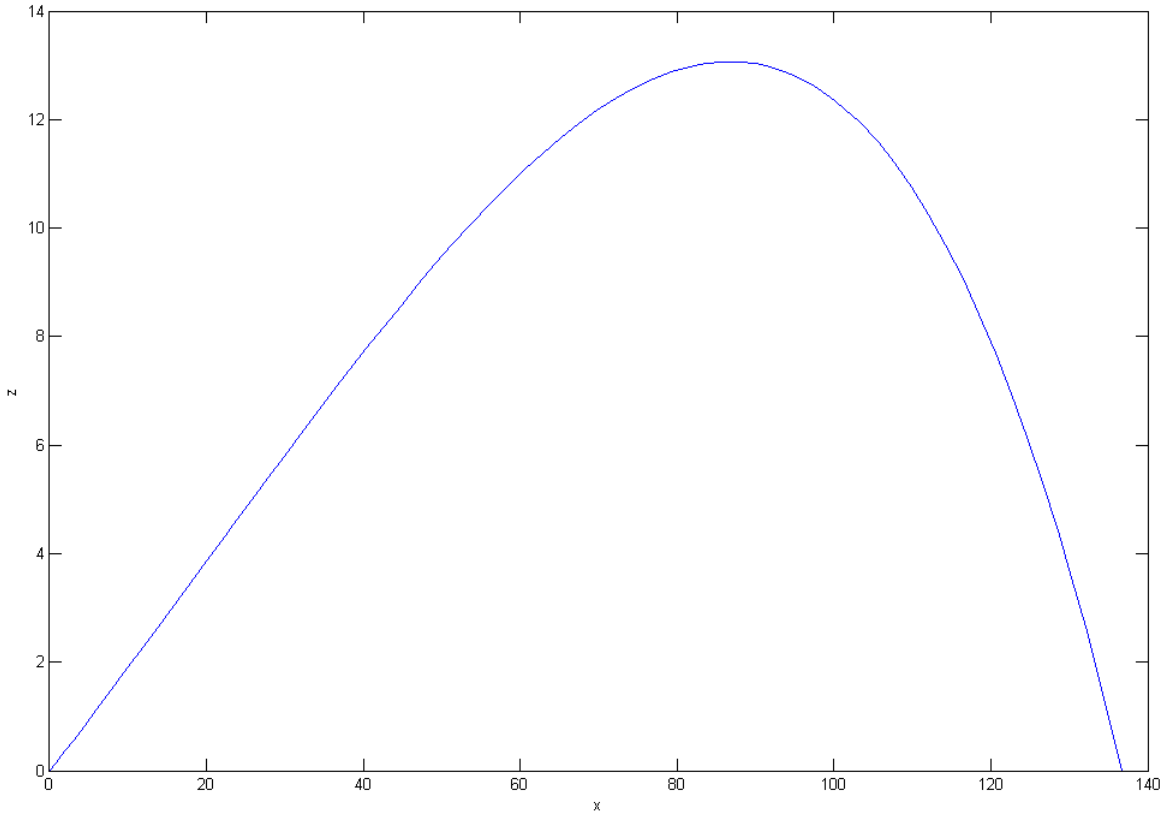


Figure 3.1: Here we plot the distance of the golf ball against the height, using the basic Robinson and Robinson model to calculate the trajectory.

In figure 3.1 we plot the range ($x$-axis) against the height of the the golf ball during the flight. There are several encouraging features within this plot: the height and range are within the bounds set by considering the ball as a projectile and completely negating the affect of drag, and the shape of the trajectory is not simply that of a parabola, implying that the lift and drag are changing how the ball flies.

In figure 3.2 we display a 3 dimensional plot of the trajectory. Here we notice that the spin of the ball influences the movement in the $y$ plane fairly considerably, adding a deviation from a standard projectile which we would not predict by projectile motion alone. This is the action of the spin on the trajectory.

## 3.2 Limitations of the Model

Whilst the model given by Robinson and Robinson (2013) is a good start, it is not without flaws. The authors themselves admit that there are a number of points where the model could potentially be improved

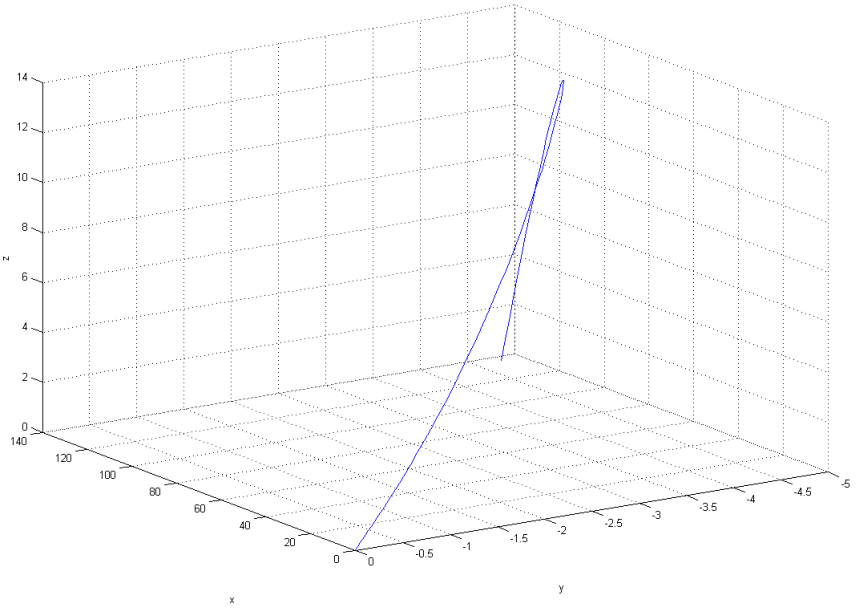


Figure 3.2: A 3D plot of the same model as Figure 3.1, showing the deviation due to the spin of the ball in this model.

- The model only takes into account a positive Magnus effect, but if the separation points were to move to a different position on the ball this form would no longer apply.
- Given the earlier analysis in this text, the constant value of $c_D$ is rather troubling.
- The form of $c_D$ and $c_L$ have no dependency on Reynolds number at all, which contradicts previous analysis.
- The spin of the ball is assumed constant throughout the flight. The authors state that in most situations the loss of spin is low enough to be ignored, citing some evidence that the ball keeps a significant proportion. This assumption is also presented in Lieberman and Smits (2001), where the simple differential equation

$$\dot{\vec{\omega}} = -0.00002\frac{\vec{\omega}v}{r}$$

  is used to model the spin decay. This constant is so small as to cause almost no change in spin over the flight, and as such we will not concern ourselves with modelling spin decay.

The authors do state, however, that building dependency on speed and spin into their model would be possible with the analysis they have performed, allowing these

limitations to be addressed without drastically changing the form of the resultant equations.

The lack of any dependency on speed is addressed within Jensen (2014) by means of dimensional analysis. Jensen uses a similar analysis to the previous section on drag to determine that if $c_L$ is independent of the Reynolds number then it cannot, by dimensionality arguments, only be a function of $\omega$. Instead, in order for the function to have some dependency on spin a possible dimensionless grouping of $r\omega/\mathbf{V}$ can be used. Jensen also suggests several other forms which $c_D$ and $c_L$ may take based solely on dimensional considerations.

Robinson and Robinson (2014) is the authors of Robinson and Robinson (2013) reply to the paper by Jensen. Robinson and Robinson state that the second constant in (3.1.4), as found from Davies (1949), is given in units of $1/(\text{rad}\,\text{s}^{-1})$, and as such cancel with the units of $\omega$ and overall give an expression which is dimensionless, as we expect $c_L$ to be from our earlier discussion. The authors go on to discuss the necessity and normality of having a multiplying constant which renders an expression dimensionally consistent, giving an example based on the spring constant from Hooke's Law.

Robinson and Robinson also give a number of other references to experimental data confirming their assumptions with regards to the dependency of lift on spin, and discuss some other alternative forms of the lift force with different dependencies on the velocity of the ball.

### 3.2.1 Comparing Trajectories with Data

In order to improve upon the model by Robinson and Robinson the first thing to do is attempt to validate the trajectories generated against data provided by The R&A, and hopefully obtain some understanding of which model assumptions are incorrect.

If we use the same initial conditions as in section 3.1.4 and plot this against a trajectory provided by The R&A using their Doppler radar system we obtain Figure 3.3. We note that the model under predicts the height and range of the ball by a considerable degree.

In Figure 3.4 a 3D plot of this data is shown. Here we see that the model initially shows good agreement with the data but as the ball approaches the top of the flight the model and the data deviate considerably from each other, with the actual trajectory

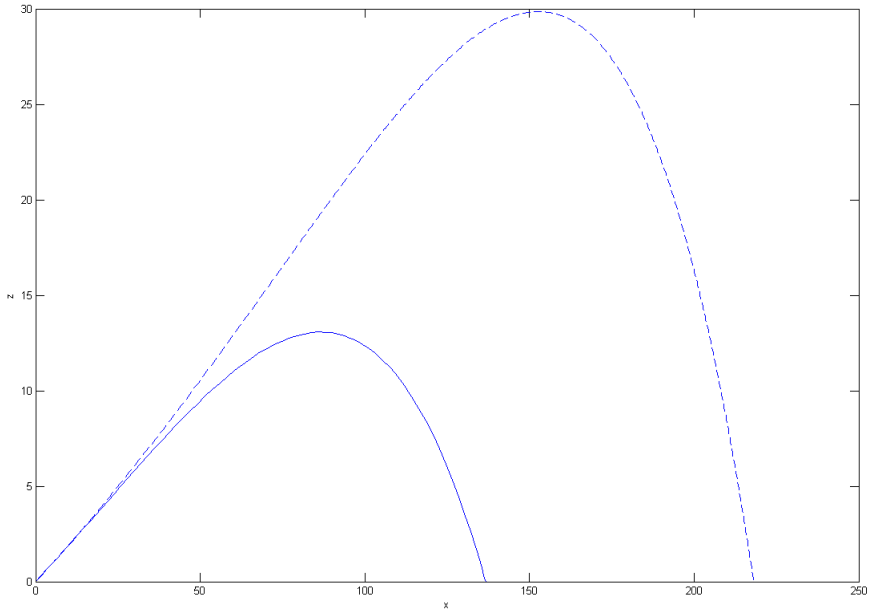


Figure 3.3: Here we plot the Robinson and Robinson model in blue against data provided by The R&A in a dashed line. The significant change in maximum height and carry of the ball highlight the fact that there are significant improvements to be made to the model.

curving back towards the $y = 0$ line. This effect is completely absent from the curve given by the Robinson and Robinson model and suggests that the drag or lift need significant changes in order to fit with the data.

One hint as to the failings of this model is to plot the speed of the projectile against the distance along the $x$-axis, as in Figure 3.5. We see that while the curves start together, they immediately deviate from each other. By $x = 50$ the Robinson and Robinson model predicts the speed to be $10\,\mathrm{m\,s^{-1}}$ less than the speed obtained from the data.

On calculating the Reynolds number for the flight, at the start of the trajectory the Reynolds number is approximately $1.6 \times 10^5$, which is just where we believe the supercritical regime begins. This would invalidate the assumption which Robinson and Robinson make that the drag is likely to be nearly constant through the entire motion of the projectile. Instead, the drag on the ball must initially be very different to the value which Robinson and Robinson assumes it to be throughout the flight. This difference accounts for the variation of the speed of the ball immediately after being hit, as the drag on the real ball is much less than the model drag, slowing the ball less and keeping the ball in the critical or supercritical Reynolds numbers for longer.

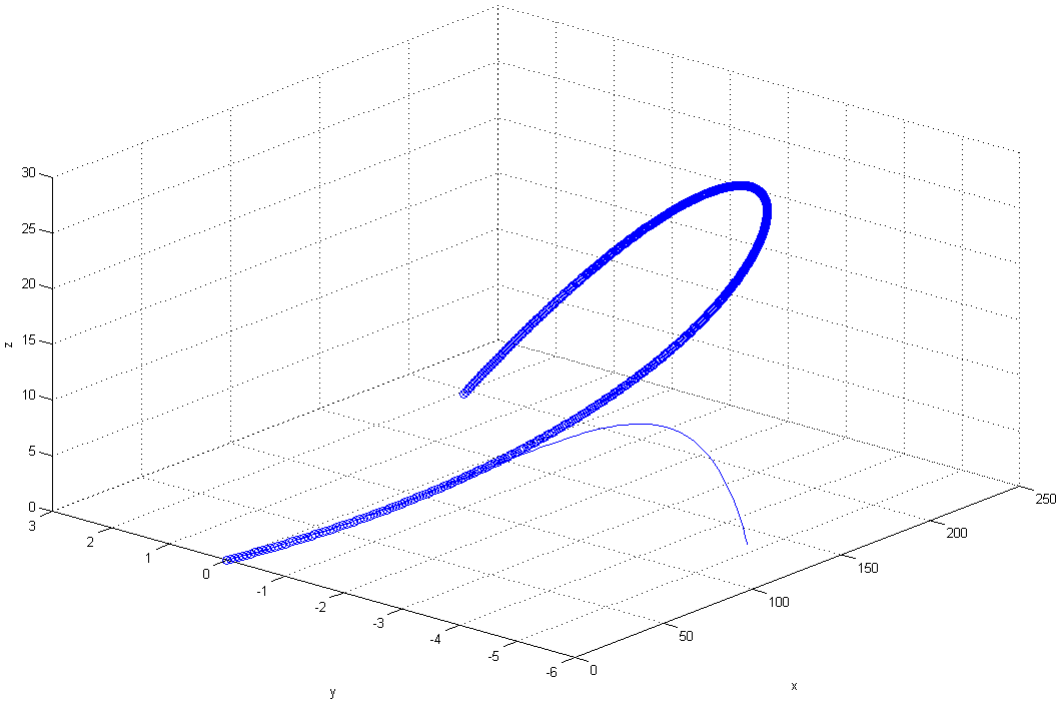


Figure 3.4: Here we plot the Robinson and Robinson model in blue against data provided by The R&A plotted with blue circles. While the model initially fits the data well, as the ball approaches the top of the flight the two curves deviate significantly.

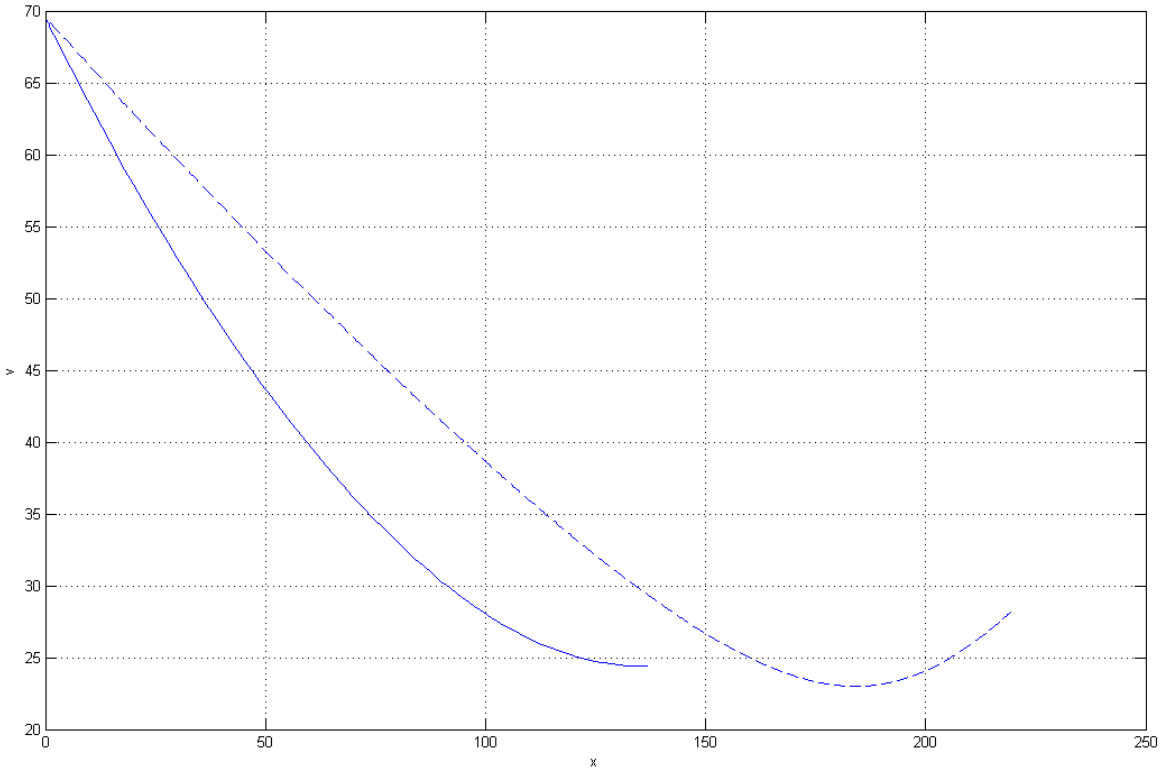


Figure 3.5: Here we plot the speed of the projectile in solid line against the speed as measured by the radar in dashed line. Note that while the curves start with the same initial condition they quickly deviate from each other.

## 3.3 Summary and Improvements

Robinson and Robinson (2013) give fairly well justified reasons to take the lift to be in the form they suggest including referencing a number of experimental results that fit well with the form they give. Thus, we will focus our investigations primarily on finding a better form for the drag function on the ball, as this will likely yield the biggest improvements to the model.

The assumption that the ball never reaches the supercritical Reynolds numbers appears, by investigation of the data above (and from other data sets obtained from The R&A) seems to be false, so finding a functional form of $c_D$ which takes into account the drag crisis for Reynolds numbers within the range encountered during golf ball flight is a good starting point for investigations. Indeed, within Lieberman and Smits (2001) the $c_D$ is also taken to be dependent on Reynolds number and other dimensionless parameters related to the spin. However, we will focus simply on dependency on Reynolds number.

Overall, the model given in Robinson and Robinson (2013) seems to be a good starting point for understanding the forces on the ball and finding trajectories, being similar in nature to the results found in previous works such as Bearman and Harvey (1976).

# Chapter 4

# Improving $c_D$

If we are to be able to estimate the trajectories based on the initial conditions successfully, we need to be able to reliably solve the forward problem[1] for the trajectory of the golf ball. In order to do this, as stated at the end of the previous chapter, we must find an improved form for $c_D$ which more accurately describes the physics which occurs during the flight of a ball.

There are a number of approaches to this, and we have attempted a few of them in our investigations in an attempt to find which of them gives the most reliable results. Any model of golf ball flight which captures the dynamics of an individual ball will have to use flight data to inform the exact parameters in a drag function for that ball. Thus, much of this chapter is also concerned with attempting to find methods of estimating the parameters for such functions given data on the flight of a particular ball.

This parameter estimation is an example of an inverse problem. Some generalities on such problems are given in the appendix.

## 4.1 Estimating $c_D$ from Experiments

As a first attempt at estimating $c_D$, we began by returning to the form given in Morrison (2010) and discussed in section 2.2.7. Recalling that we expect the dimpled surface of the golf ball to have the affect of moving the point at which the drag crisis occurs to lower Reynolds numbers, we began by taking Morrison's form for the drag and attempting to change the coefficients to "move" the drop in drag to within the range

[1] See section A.1 for a definition of a forward problem.

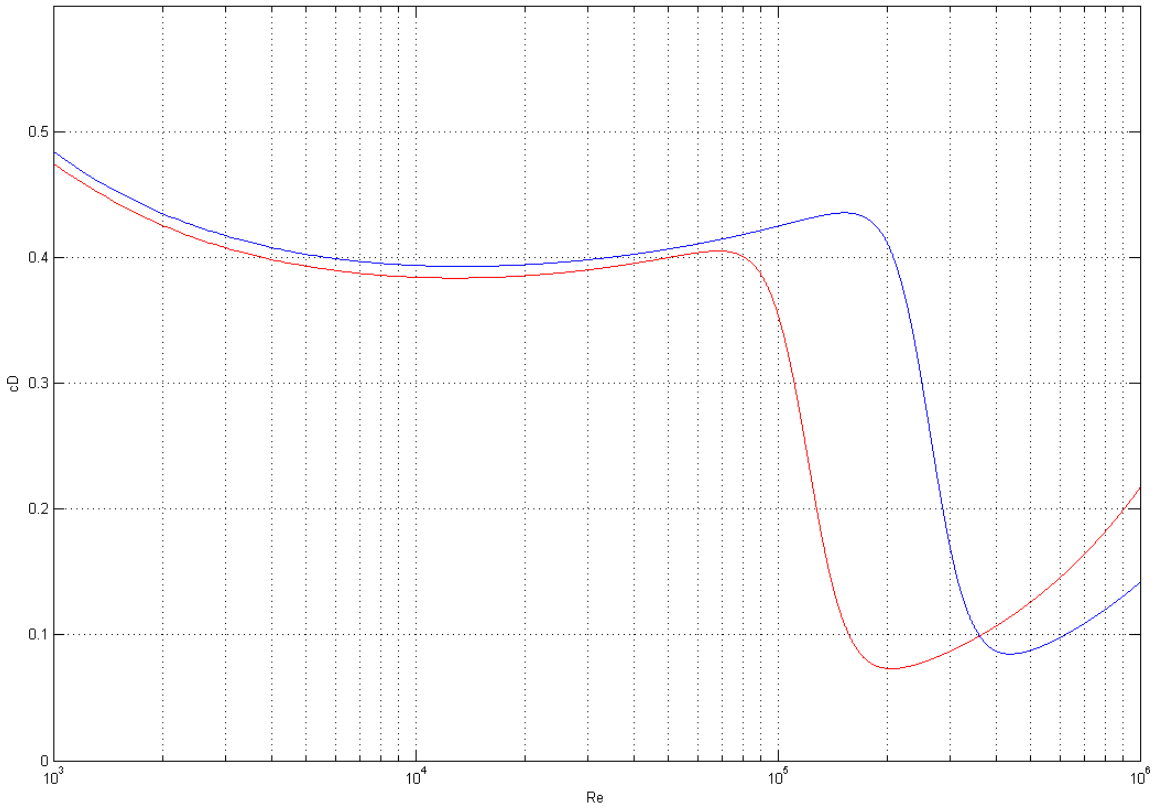


Figure 4.1: In blue is the original $c_D$ function, given in (2.2.15). In red is the modified form, (4.1.1), which takes into account the lower value of Reynolds number where the transition to lower drag occurs.

seen within experiments on golf balls.

Here, we attempt to match the function to the experimental data given in various papers which we have listed before. After some consideration, the following form of $c_D$ can be found to fit with a number of different experiments

$$c_D = \frac{24}{Re} + \frac{2.6(Re/5)}{1+(Re/5)^{1.52}} + \frac{0.38(Re/121000)^{-7.94}}{1+(Re/121000)^{-8.00}} + \frac{Re^{0.83}}{450000}. \tag{4.1.1}$$

We believe that this form captures the physics we expect to see from the golf ball better than simply taking a constant value of $c_D$ as in Robinson and Robinson (2013). Plotting the original and the modified form of $c_D$ shows how the drag has moved to within the range we expect to see.

This form has a number of limitations, but does serve to be a good initial start at working out the drag for a golf ball. The weaknesses can be summarised as

- This form of $c_D$ is constant for all types of golf balls, which we know is not the case for realistic balls, as noted in Alam et al. (2011).

- Changing this function for different balls is a matter of hand choosing coefficients in the terms of (4.1.1). This method is not at all easy to modify for other balls.

- While the form of $c_D$ is dimensionless, as we require it to be, there is no dependence on spin at all, which could be causing significant contributions to the drag.

Replacing $c_D$ in the model by Robinson and Robinson by $c_D$ as defined in (4.1.1) does make a significant change to the resultant trajectory, bringing the height of the ball much closer to the experimental trajectories and improving the carry of the ball significantly.

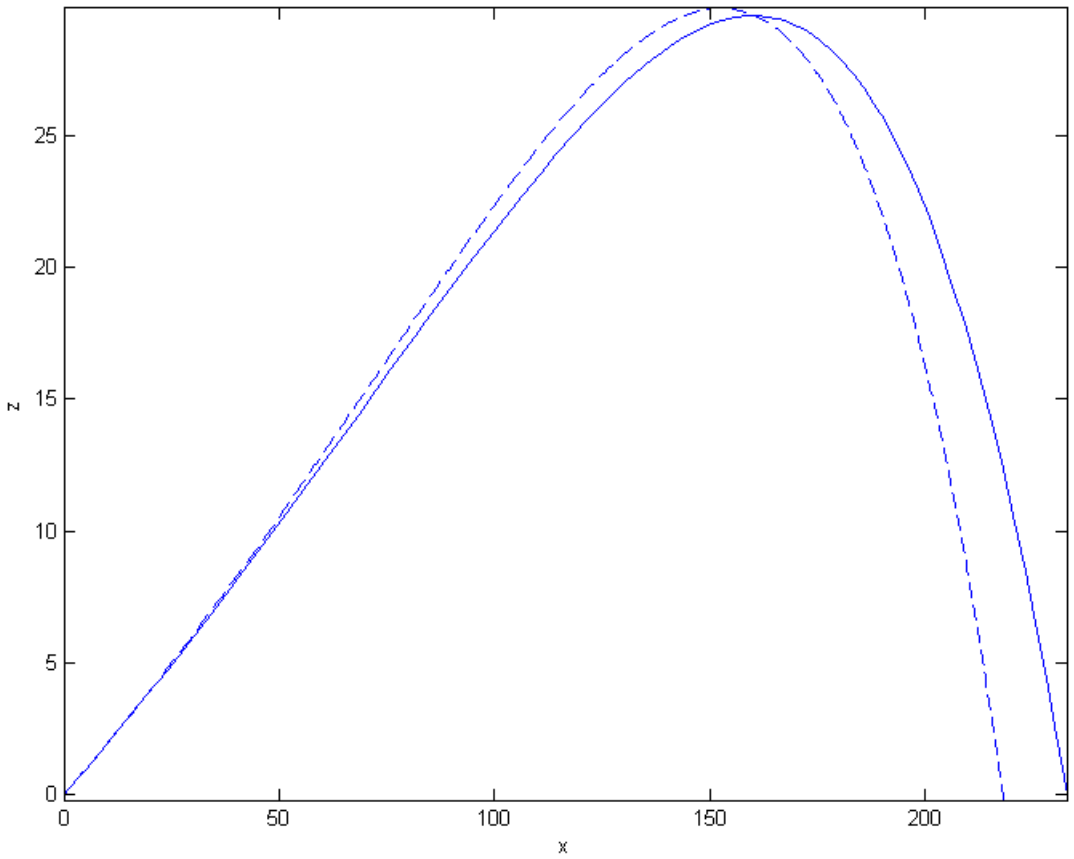


Figure 4.2: Using the modified Morrison form for $c_D$ results in a fairly accurate profile. Here the solid line is the model prediction and the dashed line is the data.

In Figure 4.2 we see that this form of the drag function brings the model and experimental results into close agreement with each other. However, viewing the trajectory in 3D reveals that while the height and carry of the ball are predicted well, the motion along the $y$ axis is not predicted as well, deviating by approximately 5m at the end of the trajectory.

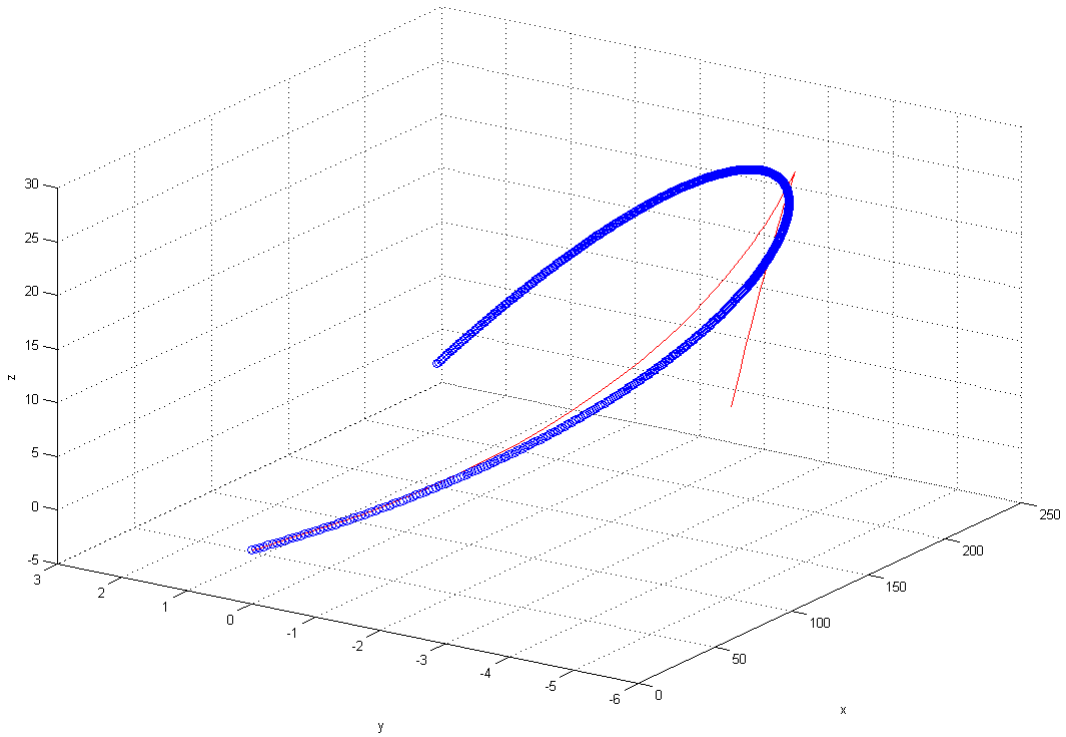


Figure 4.3: This is a 3D plot of Figure 4.2. We note that initially the predicted curve fits the data almost perfectly, being within 1m. Just before the apex of the curve however the data (plotted with circles) veers back towards the $y = 0$ line, whereas the model (in red) does not have this behaviour.

While we see good agreement between the model and the data for this data set, running the model with a different set of initial conditions and using data taken with a different ball does not yield such close agreement.

The R&A provided another data set, this time with 4 trajectories using the same ball. If we select the second trajectory from this data set to test to test this model against, with the following initial conditions

$$x = -0.112,\ y = 0.024,\ z = 0,\ v_x = 69.438,\ v_z = 9.247,\ v_y = -0.633,\ |\vec{\omega}| = 370.71,\ \theta = \frac{167\pi}{180}$$

we find (see Figure 4.4) that the trajectory does not match as closely as the previous data.

This is not that surprising however: the two separate data sets are using different balls, and thus we would expect the $c_D$ to change between the two balls.

While the modified Morrison form does give better results than simply taking $c_D$ to be constant it cannot possibly explain how $c_D$ varies for every ball. However, seeing that this form of the drag brings the model much closer in line with experimental data is encouraging, and implies that factoring in the drag crisis to the calculation of the

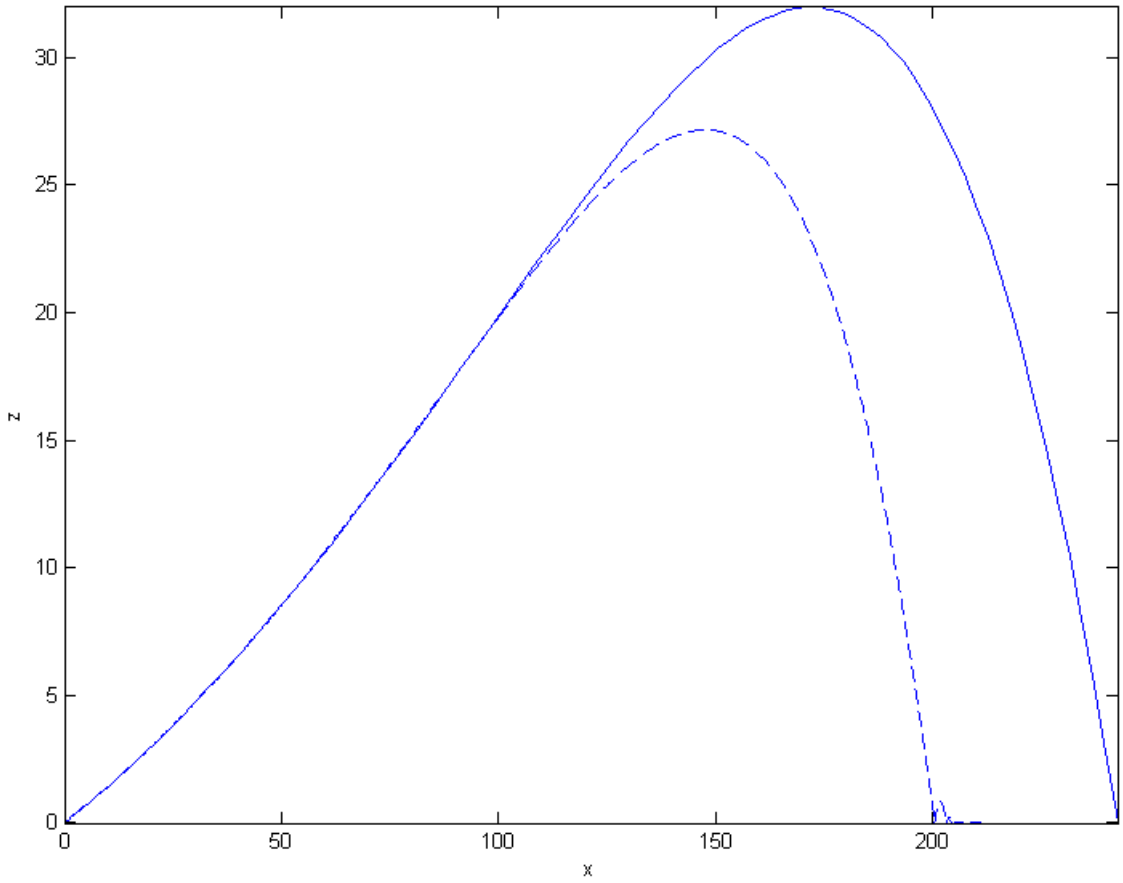


Figure 4.4: Here the dashed line is the second data set and the solid line is the model using the modified Morrison form.

model does have a major effect on the resultant trajectories as we expected it to do so.

## 4.2 Parametrising $c_D$ and $c_L$ by Non Dimensional Variables

We now attempted a different approach: following the idea of Lieberman and Smits (2001) we attempted to use the data from The R&A to estimate parameters in functions of dimensionless groupings for $c_D$ and $c_L$.

Lieberman and Smits (2001) give a number of forms for $c_D$ and $c_L$. We will use the first form given in the patent, that is

$$c_D = \bar{A} + \bar{B}Sr^2 + \bar{C}Re + \bar{D}Sr \tag{4.2.1a}$$

and

$$c_L = \hat{A} + \hat{B}Sr + \hat{C}Re^{-2} + \hat{D}Sr^2 \tag{4.2.1b}$$

where $Re$ is the Reynolds number as before, and $Sr$ is the spin ratio, defined as

$$Sr = \frac{|\vec{\omega}|D}{v}. \tag{4.2.2}$$

The spin ratio another possible dimensionless grouping, which emerges when performing the same analysis as section 2.2.4 but with $\omega$ and $\theta$ as part of the analysis. $D$ is the diameter of the golf ball.

The coefficients $\bar{A}, \bar{B}, \bar{C}, \bar{D}, \hat{A}, \hat{B}, \hat{C}, \hat{D}$ are to be determined using the data. In order to do this, we use a non linear least squares method (see appendix A.2) to fit the parameters within the model to the data set at hand.

In order to solve the problem we must specify an initial guess for the coefficients, before allowing the least squares algorithm to refine the parameters. The values for the guesses were found by simply hand optimizing the functions based on typical speeds and spins for golf balls, changing the coefficients until the values of $c_D$ and $c_L$ became fairly close to the values we expect them to take from experiments.

For $c_D$ we take

$$\bar{A} = \bar{B} = \bar{C} = \bar{D} = 6 \times 10^{-6}$$

and for $c_L$ we take

$$\hat{A} = \hat{B} = \hat{C} = \hat{D} = 0.5$$

as the initial guesses.

Running these against the data provided by The R&A provides mixed results. For some trajectories, the fit is almost perfect in all three dimensions as we see in Figure 4.5 and Figure 4.6. However, when using the same ball with different initial conditions we sometimes obtain worse fits, which do not match as well as the previous data set, for example Figure 4.7. For some of the data sets the least squares algorithm with the guesses as above cannot fit the data at all, as the new values of the parameters estimated render the equations of motion impossible to integrate using the standard routines within MATLAB and the guesses must be changed to proceed with this data set. This implies that estimating $c_D$ and $c_L$ in this way is incredibly sensitive to the choice of initial conditions and can only have limited utility if a person is required to manually change the guesses to make the model work.

Additionally, when comparing the values of $\bar{A}, \bar{B}, \bar{C}, \bar{D}, \hat{A}, \hat{B}, \hat{C}, \hat{D}$ between data sets taken with the same golf ball, we do not see any regularity for the resultant values.

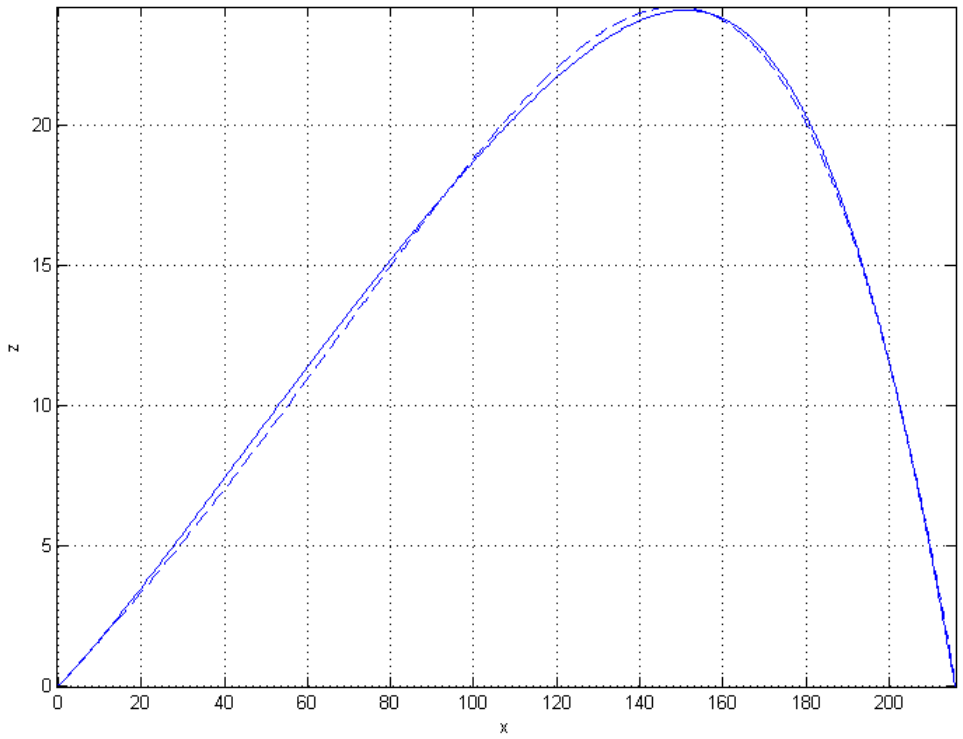


Figure 4.5: Here we plot the least squares fit using the $c_D$ and $c_L$ from Lieberman and Smits (2001) in solid line against the data set it was fitted to in dashed line. The parameter values for this trajectory are given in Table 4.1 in Data set 1.

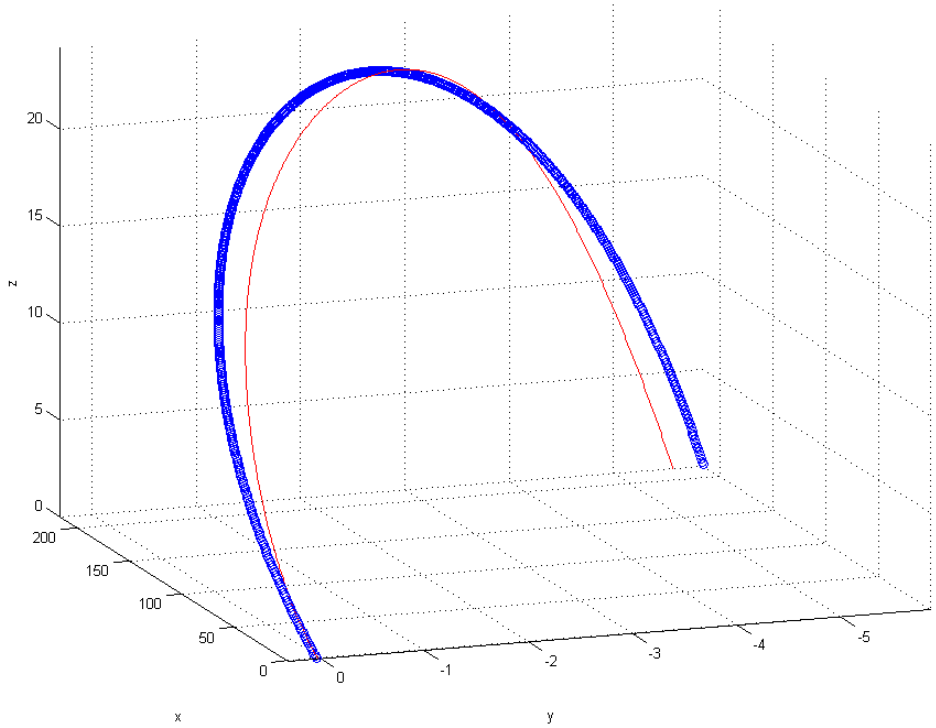


Figure 4.6: Here we plot the data and trajectory from Figure 4.5 in 3D. Note how close the red model curve has almost identical carry and shape to the thick blue data points.

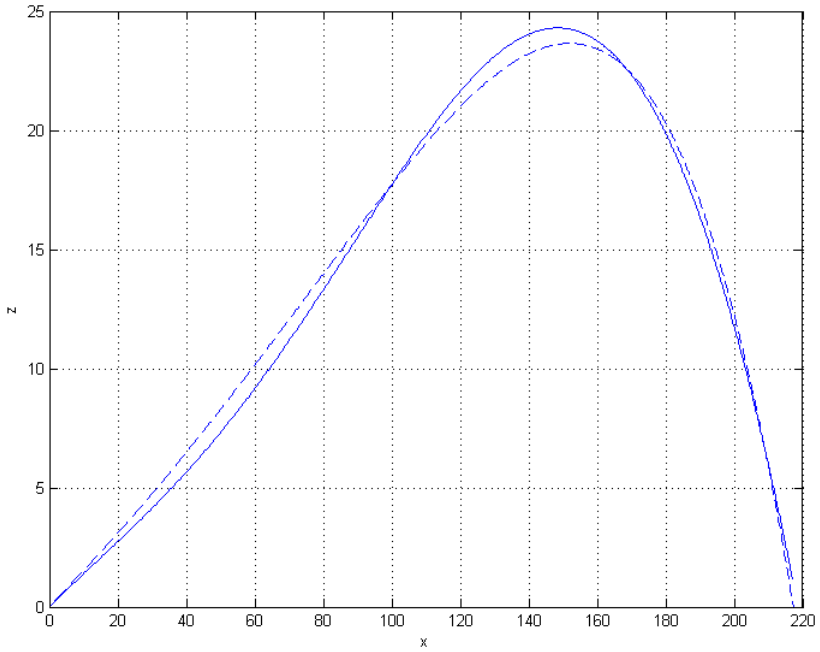


Figure 4.7: Attempting to fit the $c_D$ and $c_L$ from Lieberman and Smits (2001) works slightly less well for this trajectory than for Figure 4.5. The parameter values for this trajectory are given in Table 4.1 in Data set 3.

| Data set | $\bar{A}$ | $\bar{B}$ | $\bar{C}$ | $\bar{D}$ | $\hat{A}$ | $\hat{B}$ | $\hat{C}$ | $\hat{D}$ |
|---|---|---|---|---|---|---|---|---|
| 1 | 0.2063 | 0.2211 | -19.5001 | 0.0365 | 4.6830 | 15.9221 | $-1.4540 \times 10^{-5}$ | -15.9351 |
| 2 | 0.0697 | 1.1092 | -14.9529 | -0.8197 | -11.1921 | -24.1217 | $3.9889 \times 10^{-5}$ | 28.9117 |
| 3 | 0.3963 | -1.0174 | 0.4995 | 1.9337 | -6.3150 | -15.9492 | $2.1123 \times 10^{-5}$ | 17.3877 |
| 4 | 0.2229 | 0.0463 | 0.4999 | 0.5278 | -0.7197 | -0.0492 | $3.0765 \times 10^{-6}$ | 0.4549 |

Table 4.1: The values of the coefficients calculated using least squares for the 4 data sets with the same ball.

The R&A provided a data set using the same golf ball 4 times with 4 slightly different initial conditions. If the values of the coefficients $\bar{A}, \bar{B}, \bar{C}, \bar{D}, \hat{A}, \hat{B}, \hat{C}, \hat{D}$ are in some way physical we would expect that between the different measurements the values would stay fairly constant due to being related to the physics of the ball, rather than just fitting the data and being inconsistent between different initial conditions. However, as we can see in Table 4.1 this is not the case: the coefficients vary in sign and order of magnitude between each data set with little consistency between them.

This implies that while it is possible to fit the model data using these forms of $c_D$ and $c_L$ there is no physical data to be gained from using the least squares method here, and it would not be advisable to use the coefficients from one set of initial conditions to attempt to estimate the trajectory for another.

Since we can fit the modelled trajectories to the data using this method it is useful

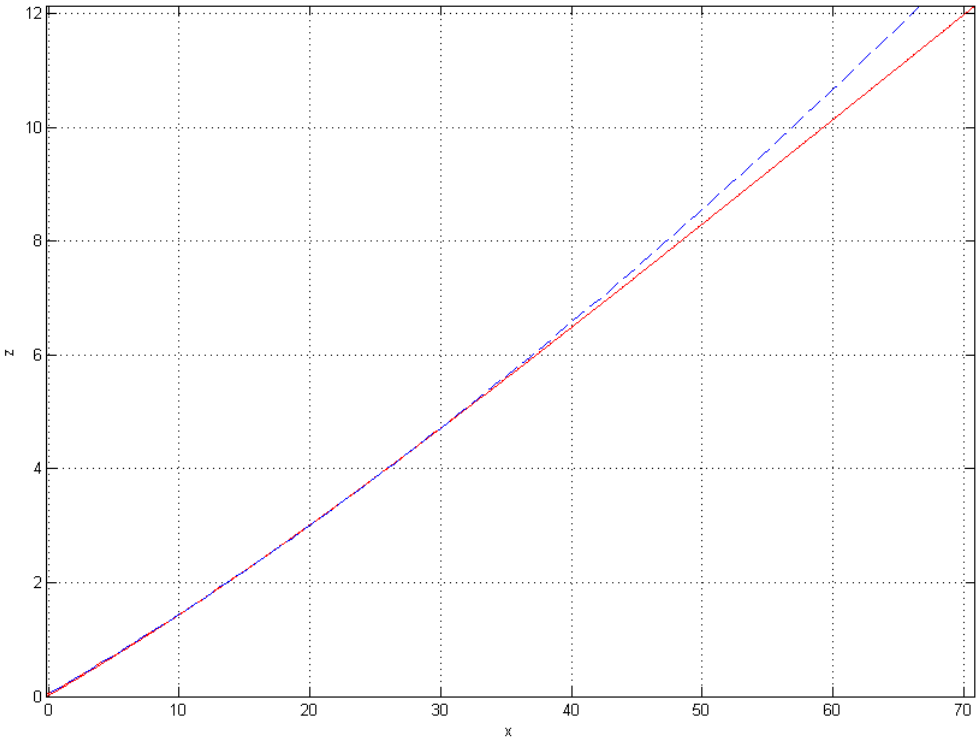


Figure 4.8: Here, we plot the data in dashed line against the least squares fitted model in red solid line. The data used in the least squares fit is from $x = 0$ to $x = 30$ and we can see that in this portion the model and the data align perfectly. After this the model and data begin to deviate slightly.

to try and see the limitations of this technique. Therefore, we then considered using only a limited portion of the data to see if the starting part of the trajectory can determine the full flight of the ball.

To do this, we simply run the same least squares method as before but with a smaller data set, over say the first 30m of the flight. We then use the predicted coefficients in $c_D$ and $c_L$ to run a full flight simulation of the ball and compare this to the full data set to ascertain how accurate this procedure is.

For the initial portion of the data the least squares matching does very well as we can see in Figure 4.8, matching the initial 30m almost perfectly. The residual between the model and the data is very small, approximately 0.0594. The values of the parameters this model produces are as follows:

$$\bar{A} = 2.2928,\ \bar{B} = -8.8290,\ \bar{C} = 0.6996,\ \bar{D} = -3.5440,$$
$$\hat{A} = -4.0220,\ \hat{B} = 2.5129,\ \hat{C} = 1.2528 \times 10^{-5},\ \hat{D} = 8.5804$$

On running the model using the values of the parameters estimated above however,

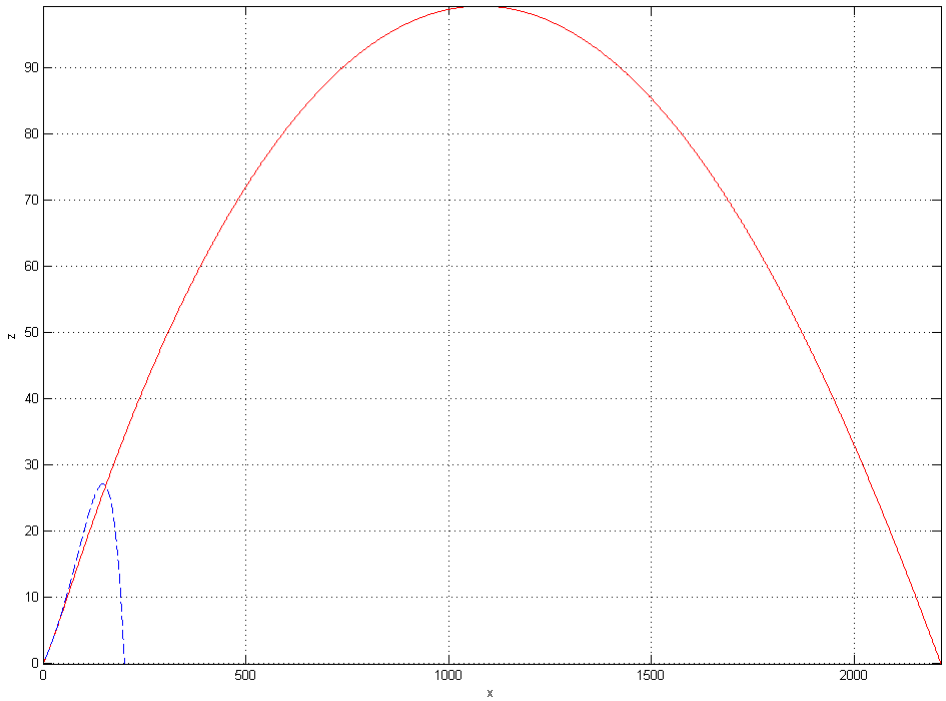


Figure 4.9: Here we run the model to the end of the trajectory using the parameters found within Figure 4.8 using least squares. The values are wildly inaccurate in both height and carry of the ball.

it quickly becomes apparent that the initially good fit is only for the starting portion of the data: the values of the parameters given massive over estimate the trajectory, with a carry in excess of 2km as we can see in Figure 4.9.

Using the least squares technique allows a good fit for the data to be found when using the whole trajectory, however estimating the parameters with a small section of the data seems to be beyond the abilities of this technique to currently estimate. It may be possible to use more sophisticated numerical techniques or to set bounds on the parameters to obtain a more realistic set of estimates for the parameters in $c_D$ and $c_L$ in this form.

## 4.3 tanh Matching

As we have seen in the previous section, using least squares estimates can produce fairly convincing fits with the experimental data we have been using. However, the physical grounding of these parameters is unknown: they are simply terms which can be selected from the dimensional analysis of the drag and lift functions and form a

dimensionless group. There is no experimental evidence that the drag or lift should take this form.

Thus, instead of attempting to use least squares on a drag form we do not have any physical basis for we will try a hybrid method between the two ideas: a drag function similar to the modified Morrison form we have in the first section but parametrised in such a way that we can use the least squares analysis to find the parameters for a particular ball.

In order to do this we approximate the drag crisis and near linear portions at the subcritical and supercritical Reynolds number by a tanh function of the form

$$c_D = a + b\tanh(-c(Re - d)). \tag{4.3.1}$$

The 4 constants $a, b, c, d$ here control the size, shape and position of the drag crisis drop. In particular

- $a$ controls the placement of the "middle" of the drag crisis drop. When $a = 0$ the drop passes through the $Re = 0$ axis.
- $b$ controls the size of the drop. When $b = 1$ and $a = 0$ the drop is from $c_D = 1$ to $c_d = -1$.
- $c$ controls how steep the drop is. As $c$ increases the drop grows asymptotically closer to a step function like drop.
- $d$ controls the placement of the drop, effectively shifting the drop to the origin of the coordinate system.

Using the knowledge of how these parameters work we can choose an initial set of $a, b, c, d$ such that the form of (4.3.1) is like that of the modified Morrison drag from section 4.1. This is simple enough that with a few minutes of trial and error the following values may be obtained

$$a = 0.24, \quad b = 0.17, \quad c = 0.00005, \quad d = 120000.$$

These values approximate the modified form of the Morrison drag very well near the drop, as we can see from Figure 4.10.

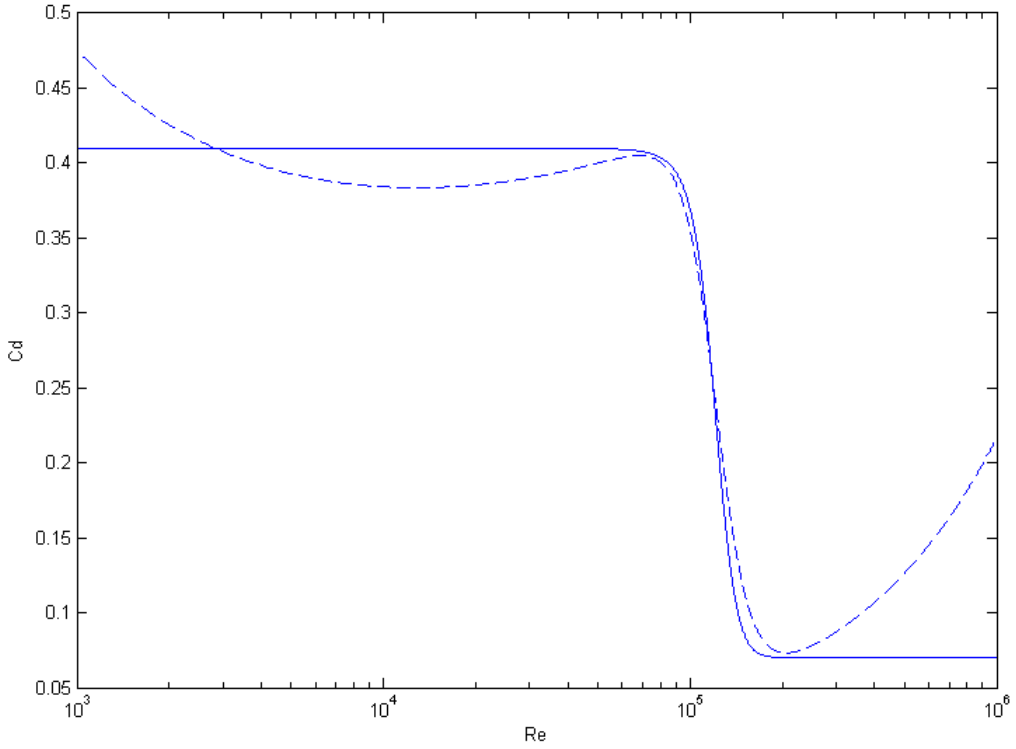


Figure 4.10: The tanh function with $a, b, c, d$ defined as above plotted in solid line against the modified drag form plotted in dashed line.

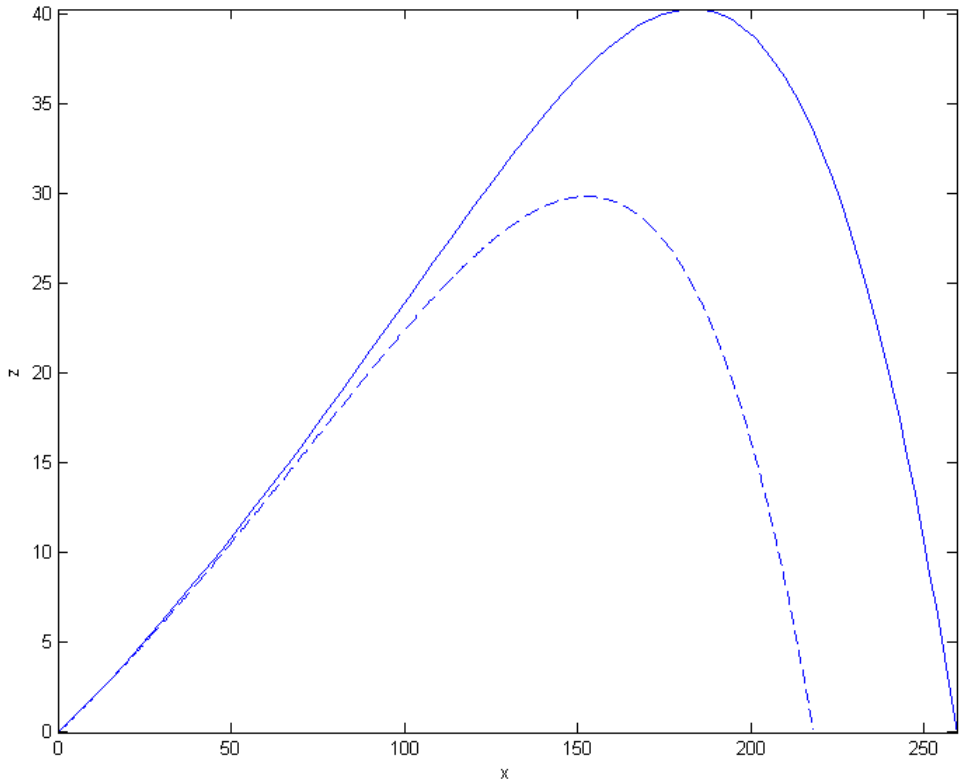


Figure 4.11: In solid line is the model for this trajectory using the tanh form for the drag function. In dashed line is the data for this trajectory.

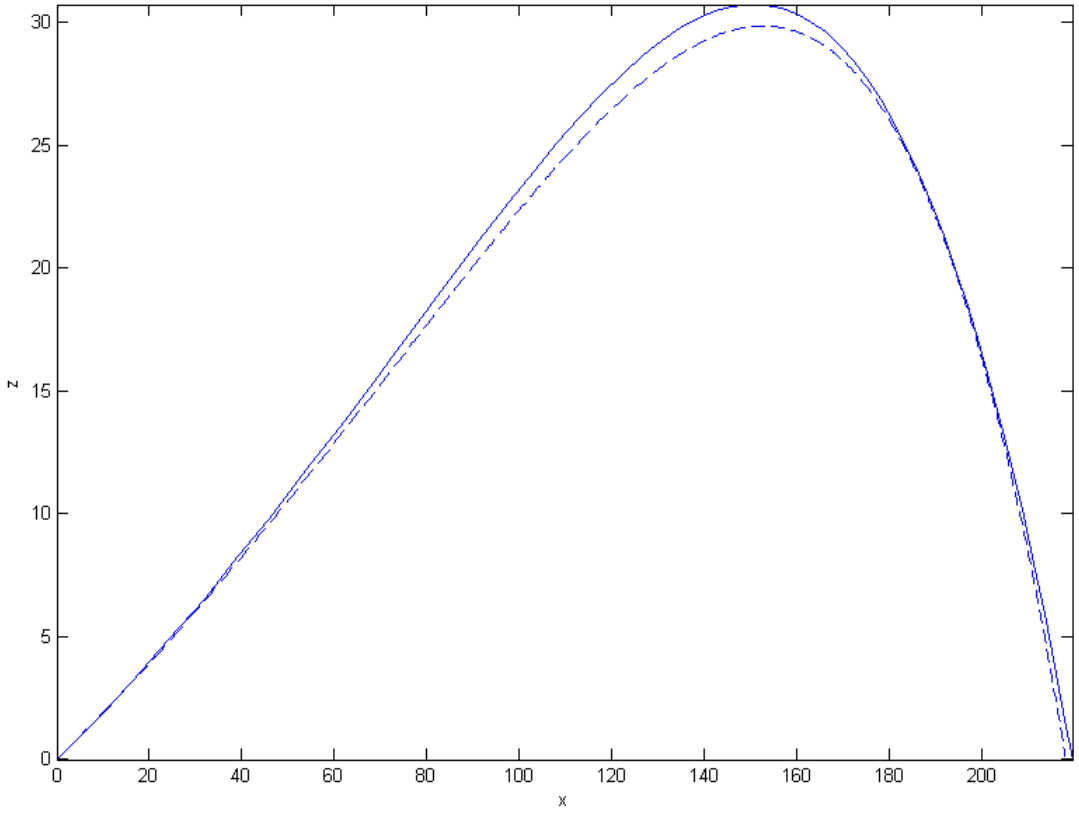


Figure 4.12: This is the same trajectory as Figure 4.11 with one of the parameters in (4.3.1) modified.

Running the model with this initial guess for the coefficients and using data set 1 we obtain a reasonable approximation to the trajectory as we can see in Figure 4.11, although not as good as we have been able to obtain with other methods.

If we then use least squares algorithm to estimate the parameters unfortunately the solution is not as easy to obtain than that using the non dimensional variables. Sometimes the solution will be obtained by the solver, but the height and carry of the ball will be greatly reduced as compared to the data, having brought the model into closer agreement with the motion along the $y$ axis at the expense of the motion along $x$ and $z$. In other cases the solver struggles to find a minimum in the parameter space at all.

This all implies that as with the previous section there is extreme sensitivity to the choice of initial guess for the coefficients in (4.3.1). For example, if we change $d$ in the initial guess from 120000 to 133000 and leave all the other parameters the same, we find a much closer fit to the data as we can see in Figure 4.12.

There are ways to proceed from here: we could constrain the problem to be within

certain ranges of parameters. However, in doing this we will inevitably lose some predictive power of the model to detect the physical characteristics of the golf ball as we desire.

## 4.4 Summary

Using least squares and more generally inverse problems techniques to estimate the parameters in the drag and lift functions for golf balls shows great promise, however we have not been able to adequately solve this problem within this project. Continuing this work requires a more thorough consideration of how to correctly estimate the parameters using inverse problems techniques.

The methods presented in this chapter do show promise however: we can improve the model beyond the assumptions of Robinson and Robinson (2013) as we hoped. These open new directions which modelling golf ball flight can continue into in the future.

# Chapter 5

# Conclusions

In this project, we have primarily strived to understand the underlying physics which affects the flight of a golf ball. In doing so we have been lead to consider the drag and lift functions in depth, as these functions contain much of the subtlety that makes golf into such a popular game for people all over the world.

The model we have developed, and the forms of $c_D$ and $c_L$, show much promise for improvement in the future.

## 5.1 Possible Future Work

# Appendix A

# Inverse Problems and Least Squares

## A.1 Inverse Problems

Tarantola (2005); Tarantola and Valette (1982)

## A.2 Least Squares

### A.2.1 Guass-Newton Method

### A.2.2 Levenberg-Marquardt Algorithm

Pujol (2007)

### A.2.3 Trust Region Method

Kelley (1999)

## A.3 Well Posedness and Regularization

Fang (2004)

# Bibliography

F. Alam, T. Steiner, H. Chowdhury, H. Moria, I. Khan, F. Aldawi, and A. Subic. A study of golf ball aerodynamic drag. *Procedia ...*, 13:226–231, 2011. doi: 10.1016/j.proeng.2011.05.077. URL http://www.sciencedirect.com/science/article/pii/S187770581100991X.

J. D. Anderson. *Fundamentals of aerodynamics*. McGraw-Hill, 1985. ISBN 0071289089.

K. Aoki, K. Muto, and H. Okanaga. Aerodynamic characteristics and flow pattern of a golf ball with rotation. *Procedia Engineering*, 2(2):2431–2436, June 2010. ISSN 18777058. doi: 10.1016/j.proeng.2010.04.011. URL http://linkinghub.elsevier.com/retrieve/pii/S1877705810002651.

P. W. Bearman and J. K. Harvey. Golf ball aerodynamics. *The Auronautical Quarterly*, 27:112–122, 1976. URL http://scholar.google.com/scholar?hl=en&btnG=Search&q=intitle:Golf+ball+aerodynamics#0.

N. Beratlis, K. Squires, and E. Balaras. Numerical investigation of magnus effect on dimpled spheres. *Journal of Turbulence*, 13(June 2014):N15, 1 2012. ISSN 1468-5248. URL http://www.tandfonline.com/doi/abs/10.1080/14685248.2012.676182.

J. M. Davies. The aerodynamics of golf balls. *Journal of Applied Physics*, 20(9): 821–828, 1949.

Q. Fang. Distinctions between LevenbergMarquardt method and Tikhonov regularization. *Dartmouth College Publication*, pages 1–7, 2004. URL http://bbs.dartmouth.edu/~fangq/blog/doc/math/LM_Tik.pdf.

J. Jensen. Comment on 'the motion of an arbitrarily rotating spherical projectile and

its application to ball games'. *Physica Scripta*, 89(6):067001, 6 2014. ISSN 0031-8949. URL http://iopscience.iop.org/1402-4896/89/6/067001.

C. T. Kelley. *Iterative methods for optimization*. SIAM, Philadelphia, 1999. ISBN 0898714338.

J. R. Kensrud and L. V. Smith. In situ drag measurements of sports balls. *Procedia Engineering*, 2(2):2437–2442, June 2010. ISSN 18777058. doi: 10.1016/j.proeng.2010.04.012. URL http://linkinghub.elsevier.com/retrieve/pii/S1877705810002663.

A. Kharlamov, Z. Chara, and P. Vlasak. Magnus and drag forces acting on golf ball. *Colloquium fluid dynamics, October*, (1959):1–9, 2007. URL http://www.it.cas.cz/files/fluid-dynamics-2007/033-Kharlamov-PT.pdf.

T. Kray, J. Franke, and W. Frank. Magnus effect on a rotating sphere at high Reynolds numbers. *Journal of Wind Engineering and Industrial Aerodynamics*, 124:46–53, Nov. 2012. ISSN 01676105. doi: 10.1016/j.jweia.2013.10.010. URL http://linkinghub.elsevier.com/retrieve/pii/S0167610512002097http://linkinghub.elsevier.com/retrieve/pii/S0167610513002328.

J. Leong and C. Lin. Effects of golf ball dimple configuration on aerodynamics, trajectory, and acoustics. *Journal of flow visualization and image ...*, 2007. URL http://www.dl.begellhouse.com/journals/52b74bd3689ab10b,622ede1536cd09e2,1d6f10f3366ac391.html.

B. Lieberman and A. Smits. Method for determining coefficients of lift and drag of a golf ball. *US Patent 6186002*, 2001. URL http://www.google.com/patents/US6186002.

J. Martin, L. V. Smith, and J. R. Kensrud. Drag on sports balls using Doppler radar. *Procedia Engineering*, 34(1):134–139, Jan. 2012. ISSN 18777058. doi: 10.1016/j.proeng.2012.04.024. URL http://linkinghub.elsevier.com/retrieve/pii/S1877705812016372.

T. Misic, M. Najdanovic-Lukic, and L. Nesic. Dimensional analysis in physics and the buckingham theorem. *European Journal of Physics*, 31(4):893, 2010. URL http://stacks.iop.org/0143-0807/31/i=4/a=019.

F. Morrison. Data correlation for drag coefficient for sphere. *Michigan Technology University, Houghton, MI*, 6(April):1–2, 2010. URL http://www.chem.mtu.edu/~fmorriso/DataCorrelationForSphereDrag2013.pdf.

T. Naruo and T. Mizota. The Influence of Golf Ball Dimples on Aerodynamic Characteristics. *Procedia Engineering*, 72:780–785, 2014. ISSN 18777058. doi: 10.1016/j.proeng.2014.06.132. URL http://www.sciencedirect.com/science/article/pii/S1877705814006481.

A. R. Penner. The physics of golf. *Reports on Progress in Physics*, 66(2):131–171, 2003. URL http://iopscience.iop.org/0034-4885/66/2/202/.

J. Pujol. The solution of nonlinear inverse problems and the Levenberg-Marquardt method. *Geophysics*, 72(4), 2007. URL http://library.seg.org/doi/abs/10.1190/1.2732552.

G. Robinson and I. Robinson. The motion of an arbitrarily rotating spherical projectile and its application to ball games. *Physica Scripta*, 88(1):018101, July 2013. ISSN 0031-8949. doi: 10.1088/0031-8949/88/01/018101. URL http://iopscience.iop.org/1402-4896/88/1/018101.

G. Robinson and I. Robinson. Reply to comment on 'the motion of an arbitrarily rotating spherical projectile and its application to ball games'. *Physica Scripta*, 89(6):067002, 6 2014. ISSN 0031-8949. URL http://iopscience.iop.org/1402-4896/89/6/067002.

A. Ruban and J. Gajjar. *Fluid Dynamics I.* Oxford University Press, 1 edition, 2014. ISBN 978-0-19-968173-0.

H. Schlichting. *Boundary layer theory.* McGraw-Hill, 1968.

W. R. Sears. *Introduction to Theoretical Aerodynamics and Hydrodynamics.* American Institute of Aeronautics and Astronautics, 2011. ISBN 1600867731.

J. Seifert. A review of the Magnus effect in aeronautics. *Progress in Aerospace Sciences*, 55:17–45, Nov. 2012. ISSN 03760421. doi: 10.1016/j.paerosci.2012.07.001. URL http://linkinghub.elsevier.com/retrieve/pii/S0376042112000656.

C. Smith, N. Beratlis, E. Balaras, K. Squires, and M. Tsunoda. Numerical investigation of the flow over a golf ball in the subcritical and supercritical regimes. *International Journal of Heat and Fluid Flow*, 31(3):262–273, June 2010. ISSN 0142727X. doi: 10.1016/j.ijheatfluidflow.2010.01.002. URL http://linkinghub.elsevier.com/retrieve/pii/S0142727X10000147.

A. Smits and S. Ogg. Golf ball aerodynamics. *The Engineering of Sport*, 2004. URL http://scholar.google.com/scholar?hl=en&btnG=Search&q=intitle:Golf+Ball+Aerodynamcs#2.

A. Tarantola. *Inverse problem theory and methods for model parameter estimation*. 2005. ISBN 0898715725. URL http://epubs.siam.org/doi/book/10.1137/1.9780898717921.

A. Tarantola and B. Valette. Generalized nonlinear inverse problems solved using the least squares criterion. *Reviews of Geophysics*, 20(2):219–232, 1982. URL http://onlinelibrary.wiley.com/doi/10.1029/RG020i002p00219/full.

H. Young and R. Freedman. *University Physics*. Addison Wesley, 12 edition, 2008. ISBN 0321501306.